UNIVERSITAT RAMON LLULL

DOCTORAL THESIS

Title **Micro and nanostructures replication via injection moulding**

Presented by **Jordi Pina Estany**

Centre **IQS School of Engineering**

Department **d'Enginyeria Industrial**

Directed by **Prof. Dr. Andrés-Amador García Granada**

"The value of this work lays merely on the large scale difference between us and the studied entities."

The author

Universitat Ramon Llull (URL)

Abstract

Institut Químic de Sarrià (IQS)
Department of Industrial Engineering

Doctor of Philosophy

Micro and nanostructures replication via injection moulding

by Jordi Pina Estany

Since polystyrene and PVC were discovered at the beginning of the 20th century, plastics have revolutionized our daily lives. The 250 millions of tonnes that are manufactured each year are used in a wide field of applications like packaging, building and construction, transportation, medical, electronics, etc.

In a similar way, nanotechnology is called to lead a disruptive change on the 21th century. Since nanotechnology emerged as a science in the 1980s, a wide field of applications has appeared in different areas like lab-on-chips devices, surfaces with self-cleaning capabilities, antimicrobial surfaces, optical applications, etc.

Currently, nanotechnology is jumping from the research area to the mass production industry. To do so, plastic appears to be a suitable material for its low cost, easiness to manufacture and interesting properties like high strength-to-weight ratio, durability, corrosion resistance, transparency, etc.

This thesis studies in detail how injection moulding manufacturing technique can be used for manufacturing plastic parts with micro and nanostructured areas. Computational Fluid Dynamics and Molecular Dynamics simulation methods are used to quantify the process and geometrical factors that effect the replication. From the experimental point of view, in a common work between IQS (Ramon Llull University), CSIC and Flubetech, plastic is injected in moulds with nanostructured areas and an Atomic Force Microscope is used for quantifying the effect of temperature, filling time, polymer charge and nanoscale geometries in the replication of nanocavities. Finally, SEAT and IQS joined efforts to develop an industrial application consisting into an improve of light homogeneity through the nanotexturising of a surface, obtaining a costs reduction and a better efficiency than the currently used methods for lighting headlamps and rear lights.

Universitat Ramon Llull (URL)

Abstract

Institut Químic de Sarrià (IQS)
Department of Industrial Engineering

Doctor of Philosophy

Micro and nanostructures replication via injection moulding

by Jordi Pina Estany

Desde el descubrimiento del poliestireno y el PVC a principios del siglo XX, los plásticos han revolucionado nuestro día a día. Las 250 millones de toneladas que se fabrican cada año se utilizan en un ámplio abanico de aplicaciones como los embalajes, la construcción, los transportes, la medicina, la electrónica, etc.

De una forma parecida, se prevé que la llegada de la nanotecnología sea un cambio disruptivo del siglo XXI. Desde que la nanotecnología nació como ciencia en los años 80, han aparecido distintas aplicaciones en distintos sectores como los laboratorios en chips, las superfícies autolimpiantes, las superfícies antimicrobios, aplicaciones ópticas, etc.

Actualmente, la nanotecnología está saltando desde los centros de investigación a la industria. Para conseguir este salto, el plástico parece ser un material adecuado debido a su bajo coste, fácil fabricación y propiedades interesantes como su alta resistencia aún y su bajo peso, la resistencia a la corrosión, la transparencia, etc.

Esta tesis estudia en detalle como la inyección de plástico se puede usar para fabricar piezas de plástico con zonas nanoestructuradas. La dinámica de fluidos computacional y la dinámica molecular se utilizan para cuantificar los parámetros de proceso y geométricos que afectan a la replicación. Desde el punto de vista experimental y en un trabajo conjunto entre IQS (Universidad Ramon Llull), CSIC y Flubetech, se inyecta plástico en moldes con superfícies nanoestructuradas y se analiza con un microscopio de fuerzas atómica el efecto en la replicación de la temperatura, el tiempo de llenado, la carga de polímero y la geometría de la nanocavidad. Para acabar, SEAT y IQS han unido esfuerzos para desarrollar una aplicación industrial centrada en la mejora de la homogeneidad lumínica mediante el nanotexturizado de una superficie, obteniendo así un método más económico y más eficiente que los métodos usados actualmente en iluminación de faros o pilotos.

Universitat Ramon Llull (URL)

Abstract

Institut Químic de Sarrià (IQS)
Department of Industrial Engineering

Doctor of Philosophy

Micro and nanostructures replication via injection moulding

by Jordi Pina Estany

Des del descobriment del poliestirè i el PVC a principis del segle XX, els plàstics han revolucionat el nostre dia a dia. Les 250 milions de tones que es fabriquen cada any s'utilitzen en un ampli ventall d'aplicacions com l'embalatge, la construcció, el transport, la medicina, l'electrònica, etc.

D'una forma similar, es preveu que la nanotecnologia sigui una innovació disruptiva el segle XXI. Des que la nanotecnologia va néixer com a ciència als anys 80, han aparegut un ampli ventall d'aplicacions com els xips en laboratoris, les superfícies amb propietats d'autoneteja, les superfícies antimicrobianes, aplicacions òptiques, etc.

Actualment, la nanotecnologia està saltant des dels centres de recerca cap a la indústria. Per fer això, el plàstic sembla ser un material adequat gràcies al seu baix cost, la fàcil fabricació i les propietats interessants com l'alta resistència tot i el baix pes, la durabilitat, la resistència a la corrosió, la transparència, etc.

Aquesta tesi estudia en detall com l'injecció de plàstic es pot utilitzar per fabricar peces de plàstic amb àrees nanoestructurades. La dinàmica de fluids i la dinàmica molecular s'utilitzen per quantificar els paràmetres de procés i geomètrics que afecten la replicació. Des d'un punt de vista experimental i dins d'un marc de treball comú entre IQS (Universitat Ramon Llull), CSIC i Flubetech, s'injecta plàstic en motlles amb zones nanoestructurades i s'utilitza un microscopi de forces atòmiques per quantificar l'efecte en la replicació de la temperatura, el temps d'omplerta, la càrrega de polímer i la geometria de la nanocavitat. Per acabar, SEAT i l'IQS han unit esforços per desenvolupar una aplicació industrial centrada en la millora de l'homogeneïtat lumínica mitjançant el nanotexturitzat d'una superfície, s'ha obtingut d'aquesta manera un mètode més econòmic i eficient que els utilitzats actualment en l'il·luminació de fars i pilots.

Acknowledgements

I express my thanks to my parents (Magí Pina and Carme Estany) and brother (Carles Pina) for giving me their support during these years. An special acknowledgement is for my wife, Irene Solanich, for her support and the language proofreading she pursued.

I am also grateful to IQS for providing me with all the necessary facilities. In particular to Dr. Carles Colominas and Dr. Josep Maria Puigoriol and my PhD Director Dr. Andrés García for his expert, sincere and valuable guidance and encouragement.

I would also like to acknowledge the members of CSIC with whom a large experimental part, conference travels and two papers were shared: Jordi Fraxedas, Francesc Pérez Murano, Dani Ruso, Olga Muntada and Jordi Llobet. The work between IQS, CSIC and Flubetech among others was founded through the european project aim4np, which served as a kickoff of this thesis.

I also appreciate the support of SEAT, and specially Ernest Corull, for making possible the conversion of all the theoretical and laboratory experimentals into an industrial application.

Contents

List of Figures

Only the figures used in the thesis specific sections are summarized. The figures of the "Publications derived from this thesis" section are not included.

List of Tables

Only the tables used in the thesis specific sections are summarized. The tables of the "Publications derived from this thesis" section are not included.

List of Abbreviations

AFM	**A**tomic Force **M**ycroscope
CFD	**C**omputational **F**luid **D**ynamics
CW laser	**C**ontinuous **W**ave laser
DOE	**D**esign **of** **E**xperiments
DP	**D**egree of **P**olymerization
FIB	**F**ocused **I**on **B**eam
FISH	**F**luorescense **in** **s**itu **h**ybridization
HTC	**H**eat **T**ransfer **C**oefficient
LOC	**L**ab-**o**n-a-**c**hip
MD	**M**olecular **D**ynamics
MEMS	**m**icro**e**lectro**m**echanical **systems**
MTS	**m**icro **t**extured**s**urfaces
NEMS	**n**ano**e**lectro**m**echanical **systems**
NFT	**N**o Flow **T**emperature
NTS	**n**ano **t**extured**s**urfaces
P	**P**ressure
PC	**P**oly**c**arbonate
PMMA	**P**oly**m**ethyl**m**ethacryl**a**te
PVC	**P**oly**v**inyl **c**hloride
PE	**P**oly**e**thylene
PP	**P**oly**p**ropylene
PS	**P**oly**s**tyrene
r	**r**adius
RIE	**R**eactive-**I**on-**E**tching
SAVR	**S**urface-**a**rea-to-**v**olume-**r**atio
SEM	**S**canning Electron **M**icroscope
T	**T**emperature

Only the abbreviations used in the thesis specific sections are summarized. The abbreviations of the "Publications derived from this thesis" section are not included.

Chapter 1

Introduction

This introduction starts with an overview of the plastics and nanotechnology industries. It follows an explanation of how injection moulding can be used to merge both industries with a single purpose, i.e., the cost-effective manufacture of plastic parts with micro and nanofeatures. The experimental procedures used to engrave such features in the mould steel, replicate them in the plastic parts and measure the results are summarized in the "Experimental analysis" section. Finally, the self developed Computational Fluid Dynamics (CFD) and Molecular Dynamics (MD) mathematical models used to model the nanostructures replication are summarized in the "Simulation analysis" section.

1.1 Plastics industry

Plastics are part of our common lives since its industry was born with the invention of baquelite by Dr. Leo Baeckeland in 1907. During the last 50 years the use of plastic has raised continuously, reaching on 2013 an annual production of 299 million tons. In fact, 4% of the petroleum consumed worldwide each year is used to make plastic ([10], [11]).

Its properties like light weight, high resistance to various chemicals, thermal and electrical insulation and its wide range of colors make them suitable for different applications like packaging (39.6%), building construction (20.3%), automotive (8.5%), electrical electronics (5.6%), agriculture (4.3%) and others like consumer and household appliances, furniture, sport, etc. (21.7%). [10].

Different methods to manufacture plastic parts are available. Next, a brief exposition of the most common forms of processing plastics is shown:

- Thermoforming
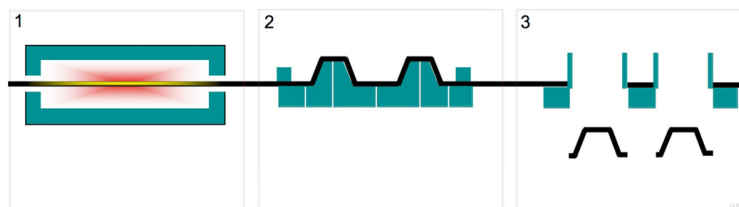
FIGURE 1.1: Thermoforming process sketch: 1) The plastic sheet is heated. 2) The sheet is formed to a specific shape in a mold. 3) The shapes are trimmed. Figure from Wikimedia Commons.

Thermoforming is a manufacturing process where a plastic sheet is heated to a pliable forming temperature, formed to a specific shape in a mold, and

trimmed to create a usable product. The sheet, or "film" when referring to thinner gauges and certain material types, is heated in an oven to a high-enough temperature that enables it to be stretched into or onto a mold and cooled to a finished shape [12]. See figure 1.1 for a sketch of the process.

- Blow molding

  Blow molding is a manufacturing process by which hollow plastic parts are formed. There are two main types of blow moulding: injection blow molding and extrusion blow molding. The blow molding process begins by melting down the plastic and forming it into a parison or in the case of injection blow molding a preform. The parison is a tube-like piece of plastic with a hole in one end through which compressed air can pass. The parison or the preform is then clamped into a mold and air is blown into it. The air pressure then pushes the plastic out to match the mold. Once the plastic has cooled and hardened the mold opens up and the part is ejected. See figure 1.2 for a sequence of images of the injection blow molding process and figure 1.3 for a sequence of the extrusion blow molding process [13].
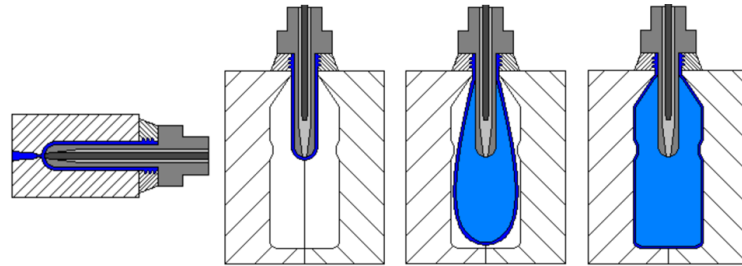
FIGURE 1.2: Injection blow molding process sequence. The preform is manufactured in a first step and blown inside a mould next. Figure from Wikimedia Commons.
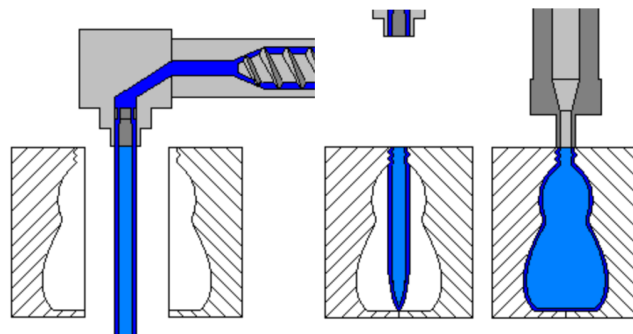
FIGURE 1.3: Extrusion molding process sequence. The parison is manufactured in a first step and blowed inside a mould next. Figure from Wikimedia Commons.

- Rotational molding

  Rotational molding, also called rotomolding or rotocast, is a thermoplastic process for producing hollow parts by placing powder or liquid resin into a hollow mold and then rotating that tool bi-axially in an oven until the resin melts and coats the inside of the mold cavity. Then the tool is cooled and the part is removed from the mold [14]. See figure 1.4 for a process diagram.
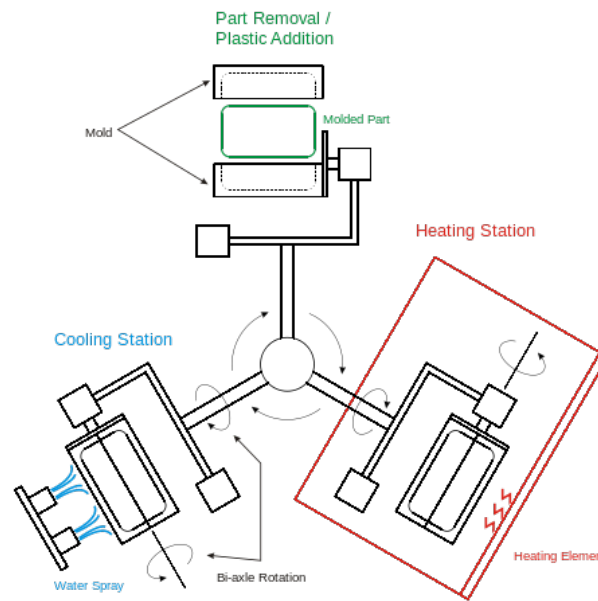
FIGURE 1.4: Rotational molding mold process diagram, the three stations are observed (plastic addition and part removal, heating station and cooling). Figure from Wikimedia Commons.

- Injection molding

  Injection molding is the plastic manufacture technology used in this thesis. Because of this, its description is specially detailed. With injection molding, granular plastic is melted and forced inside the mould cavity using a screw-type plunger. Once inside the mould cavity (the negative of the desired part), the plastic solidifies and adquires the shape of the mold (see figure 1.5).
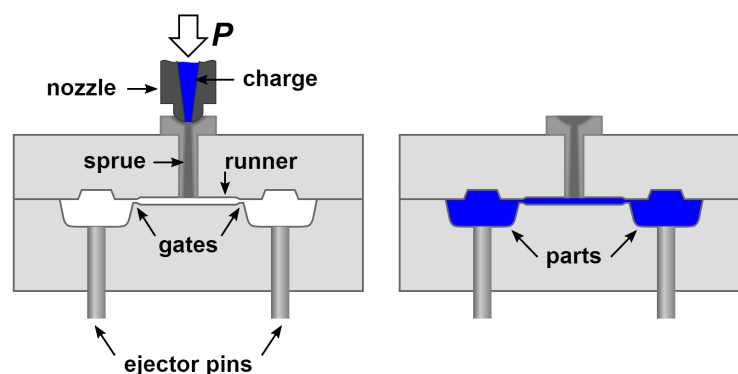
FIGURE 1.5: Simplified diagram of the injection moulding process. Figure from Wikimedia Commons.

  This process is done in machines like the sketched in figure 1.6 and is described next [15]:

  1. Clamping. Prior to the injection of the material into the mold, the two halves of the mold must first be securely closed by the clamping unit. Each half of the mold is attached to the injection molding machine and one half is allowed to slide. The hydraulically powered clamping unit
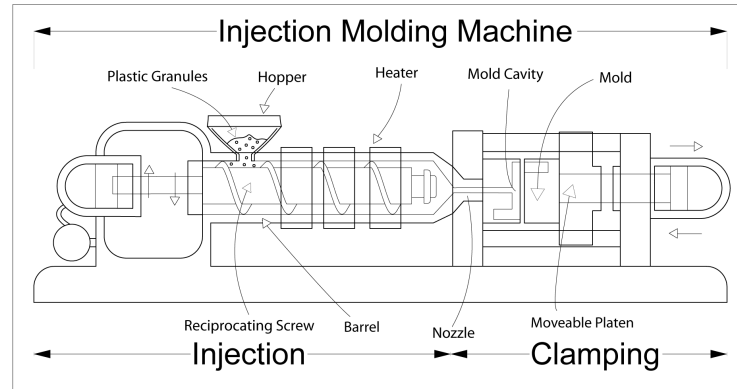
FIGURE 1.6: Moulding machine sketch. Figure from Wikimedia Commons.

pushes the mold halves together and exerts sufficient force to keep the mold securely closed while the material is injected.

2. Injection. The raw plastic material, usually in the form of pellets, is fed into the injection molding machine, and advanced towards the mold by the injection unit. During this process, the material is melted by heat and pressure. The molten plastic is then injected into the mold very quickly and the buildup of pressure packs and holds the material. The amount of material that is injected is referred to as the shot.

Normally, the moulds are warmed with hot water, however, in paper VI (Pina [4]), Heat & Cool molding system is used. With this technology, an alternating electrical current is applied to an array of inductors placed inside the steel to create an alternating magnetic field, which according to Faraday's Law induces an electric current that warms the mould due to Joule effect. This technology enables a fast heating of the mould (up to 25 ºC/s), far larger than conventional heating with water or steam (approx 10 ºC/s) and a maximum mould temperature of up to 400 ºC compared to conventional heatings of 140 ºC. See figure 1.7 for a sketch of the temperature and pressure synchronization.
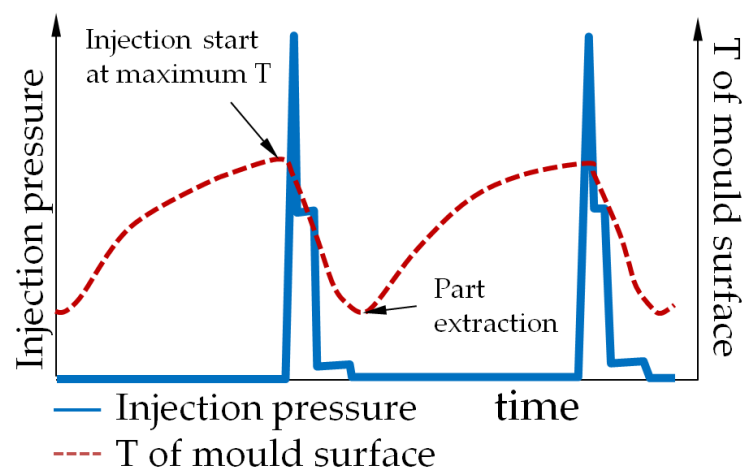
FIGURE 1.7: Heat and cool temperature profile. Own source image.

3. Cooling. The molten plastic that is inside the mold begins to cool as soon as it makes contact with the interior mold surfaces. As the plastic cools, it will solidify into the shape of the desired part. However, during cooling some shrinkage of the part may occur. The packing of material in the injection stage allows additional material to flow into the mold and reduce the amount of visible shrinkage. The mold can not be opened until the required cooling time has elapsed.

4. Ejection. After enough time has passed, the cooled part may be ejected from the mold by the ejection system, which is attached to the rear half of the mold. When the mold is opened, a mechanism is used to push the part out of the mold. Force must be applied to eject the part because during cooling the part shrinks and adheres to the mold.

   Undercuts are normally manufactured at normal scales with sliders (see figure 1.8). Even though this is possible at normal scales, nanoscale features must be demouldable in order to manufacture them through injection moulding.
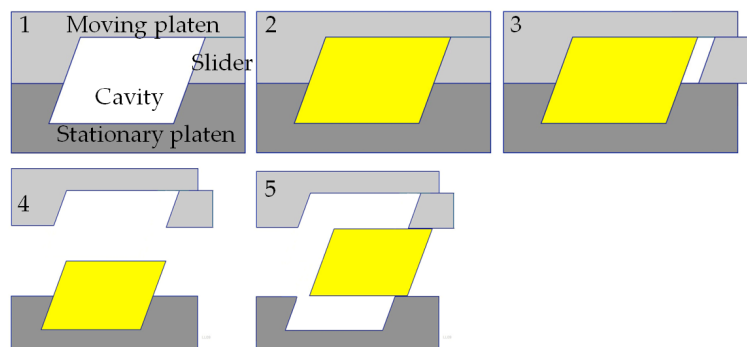
FIGURE 1.8: Slider used to demould an undercut. Image adapted from a GIF of Wikimedia Commons.

Concerning to the materials, only thermoplastics can be injected with injection moulding. Thermoplastics are plastics that become plastic on heating and harden on cooling, with the ability to repeat these processes. In this thesis PC, PMMA, PP, PS and PE are injected. Next, a brief overview of each polymer is shown:

– Polycarbonate (PC)
  The main polycarbonate material is a transparent thermoplastic produced by the reaction of bisphenol A and phosgene. The repeating monomer is depicted in figure 1.9.
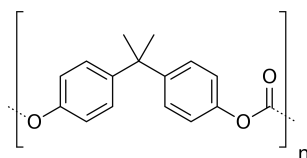
FIGURE 1.9: Repeating monomer of PC. Figure from Wikimedia Commons.

It stands out for its temperature resistance, impact resistance and optical properties such as high optical transmission in the visible range. PC is

commonly used in CDs and DVDs, cars headlamps, large water bottles placed on water coolers, noise barriers, laboratory saffety glasses, etc. Its disadvantage is its large hygroscopy, PC absorves up to a 0.2%-0.3% of humidity in equilibrium, this leads to large drying costs in order to avoid sink marks, cracks in the surface, material degradation, low viscosity, etc.

– Polymethylmethacrylate (PMMA)

PMMA, also known as acrylic or acrylic glass is a transparent thermoplastic. Chemically, it is the synthetic polymer of methyl methacrylate. The chemical structure is shown in figure 1.10.
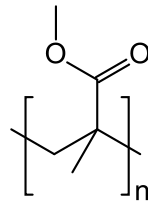
FIGURE 1.10: Repeating monomer of PMMA. Figure from Wikimedia Commons.

PMMA is an economical alternative to polycarbonate (PC) when tensile strength, flexural strength, transparency, polishability and UV tolerance are more important than impact strength, chemical resistance and heat resistance.

It is used as a transparent glass substitute in aquariums, rear lamps of automobiles, lighthouse lenses, etc. It is also used in medical applications, for example, to manufacture rigid introcular lenses which are implanted in the eye when the original lens has been removed in the treatment of cataracts. In architecture and furniture, it is used to manufacture bathtubs, shower cabin doors, door and windows profiles, etc. Greenhouses are also manufactured with PMMA because it facilitates light transmission, which helps the plants grow quicker.

– Polypropylene (PP)

Polypropylene is an addition polymer made from the monomer propylene and it results in a chain of repeating monomers like depicted in figure 1.11.
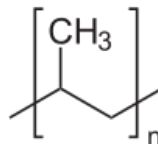
FIGURE 1.11: Repeating monomer of PP. Figure from Wikimedia Commons.

Polypropylene is used for a wide number of different products. It is used in parts that are going to have high stress, such as hinge mechanisms on water bottles and more. It is also used in manufacturing piping systems, as well as chairs, and in medical or laboratory use. The colorfastness makes it suitable in carpeting, rugs, and mats. Ropes, cable insulation, roofing membranes, storage boxes, disposable bottles, plastic pails and other items are also made using this type of plastic.

TABLE 1.1: Cost of the different polymers [9].

Polymer	Cost
PC	3.25 €/kg
PMMA	3.05 €/kg
PP	1.37 €/kg
PS	1.68 €/kg
PE	1.28 €/kg

– Polystyrene (PS)

Polystyrene is a synthetic aromatic polymer made from the monomer styrene, see figure 1.12. Polystyrene can be naturally transparent, but can be colored with colorants. It is used in protective packaging (such as CD and DVD cases), containers, lids, bottles, disposable cutlery, etc.
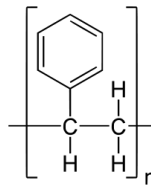
FIGURE 1.12: Repeating monomer of PS. Figure from Wikimedia Commons.

– Polyethylene (PE)

Polyethylene is the most common plastic, with an annual global production of around 80 million tonnes. Its primary use is in packaging (plastic bags, plastic films, geomembranes, containers including bottles, etc.). See figure 1.13 for an image of the repeating unit of PE.
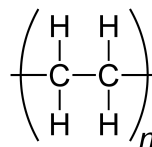
FIGURE 1.13: Repeating monomer of PE. Figure from Wikimedia Commons.

The costs of the above exposed materials is summarized in table 1.1. It is observed how PE and PP are the cheapest polymers, in comparison to PC and PMMA whose cost is above 3 €/kg.

The above cited materials are the ones used in this thesis either in the simulations or in the experimental parts. However, nearly any thermoplastic polymer can be used in injection moulding manufacturing technique. According to its viscosity, heat capacity, density and other properties the replication will be more or less successful. Even not commonly used thermoplastics are under research; for example, polylactic acid is currently under research because it is biodegradable and bioactive, with a manufacture derived from renewable resources (corn stach, cassava roots, chips or starch or sugarcane).

Even though only pure materials have been used in the present work, the appropriate use of polymer additives improve many characteristics such as durability, stiffness, clarity, weatherability, etc. For example, antioxidants scavenge peroxy radicals and decompose hydroperoxides to prevent thermal degradation of polymers. Light stabilizers provide protection against photo degradation, ultraviolet absorvers convert light energy into thermal energy, Hindered Amine Light Stabilizers scavenge radicals generated through photo degradation. Nucleating agents and clarifying agents enhance crystallization rate and improve therefore the mechanical properties, the heat distortion temperature and the transparency, they even shorten the moulding cycletime because of the improvement of crystallization temperature. Flame retardant additives, plasticisers to obtain flexibility, colourants and other additives are also commonly used in the injection moulding and the plastics industry in general.

1.2   Nanotechnology industry

Nanotechnology applications are defined as the creation and use of materials, devices and systems through the manipulation of matter at scales of less than 100 nanometers, i.e., $0.1\ \mu m$. The nanotechnology is considered to be born in the year 1959, when Richard Feynman initially designed the idea of molecular manufacturing in his speech "there is plenty of room at the bottom".

A prove of the nanotechnology industry growth is the european project aim4np. This project took place between March 2013 and August 2016 and its main deliverable was a fast robotic metrology platform to measure with nanometer resolution the nanomechanical properties of large samples in a production environment. The Workpackage assigned to IQS, CSIC and Flubetech consisted on studying how the mould roughness was replicated in the plastic parts. Once studying the roughness replication, the interest deviated to the replication of tailored structures, serving this as inspiration, first steps and finally as a true kickoff of this thesis.

What characterizes the nanotechnology is its large surface-area-to-volume ratio (SAVR), for example, an sphere has an area-to-volume ratio of $3/r$, what means that SAVR tends to infinite as the radius tends to zero. When the percentage of the surface in relation to the percentage of the volume of material becomes significant the materials change their properties. For example, nanoparticles exhibit unexpected optical properties since they are small enough to confine their electrons and produce quantum effects [16]. Gold nanoparticles melt at lower temperatures ($\approx 300^{\circ}$C for 2.5 nm size) than the gold slabs (1064 $^{\circ}$C) [17]. Solar radiation absorption can be improved by controlling the size, shape and material of the particles [18] [19] [20] [21]. Suspensions of nanoparticles are possible since the interaction of the particle surface with the solvent is strong enough to overcome density differences, which otherwise usually result in a material either sinking or floating in a liquid.

This thesis is focused in micro and nanotextured surfaces (MTS and NTS, respectively), i.e., surfaces covered with micro or nano-sized structures that can be in various forms like cones, columns, fibers, etc. With, at least, one dimension at these scales. What defines the behaviour of the NTS is, mainly, the period and the aspect ratio of the nanostructures, see figure 1.14 [22]. Kim shows in the publication "Nanostructured multifunctional surface with antireflective
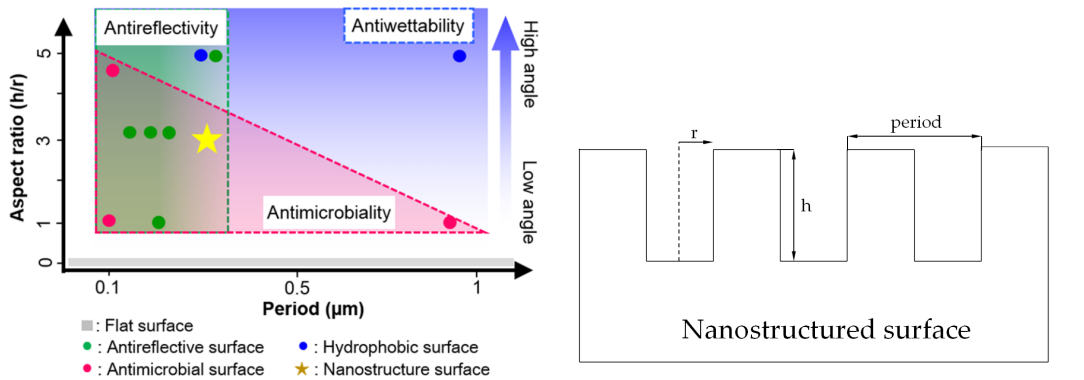
(A) Behaviour of NTS as a function of its geometry. The colored box delineates the optimal performance of each functionality reported in the literature. Figure from Kim et al. [23]

(B) Geometric parameters that define the periodic nanotextures.

FIGURE 1.14: NTS geometric parameters and their resulting functionality. Own source image.

and antimicrobial characteristics" [23] the graph of figure 1.14a were the surface behaviour is defined as a function of the nanostructure geometry, with the period and aspect ratio combinations that lead to antireflectivity, antimicrobiality and antiwettability. It is stated that a surface is antireflective when the nanotexture has a period between 0.08 and 0.3 µm, preferably with an aspect ratio of 3; antimicrobial with a period between 0.08 and 1 µm and antiwettable when the period is between 0.08 and 1 µm and the aspect ratio between 1 and 6.

Following, some of these applications are briefed along with a literature review:

– Optics

From the optical point of view, anti-reflective surfaces have been manufactured. Christiansen exposes in "Injection moulding antireflective surfaces" [24] how moulded structures of 125 nm height reduce the visible spectrum reflectance of black polypropylene from $4.5 \pm 0.5\%$ to $2.5 \pm 0.5\%$. The structures are manufactured in black silicon masters with mask-less reactive ion etching and electroplated with nickel.

Nanostructures in opaque materials that reduce the reflectance can also enhance the chroma of plastics, leading to a clearer color experience. This is studied in "Enhancing the chroma of pigmented polymers using antireflective surface structures" by Clausen et. al [25].

When studying how nanostructures affect the light properties, it is important to take into account the electromagnetic spectrum (see figure 1.15). For example, nanostructures diffract the light when their size is similar to the the visible range (400 to 700 nm aprox.).

In paper VI (Pina [8]) an optical application with industrial purposes is shown. Indeed, homogeneous and heterogeneous diffusion of the light is obtained along with the projection of nanoscaled geometrical shapes.

– Fluidics
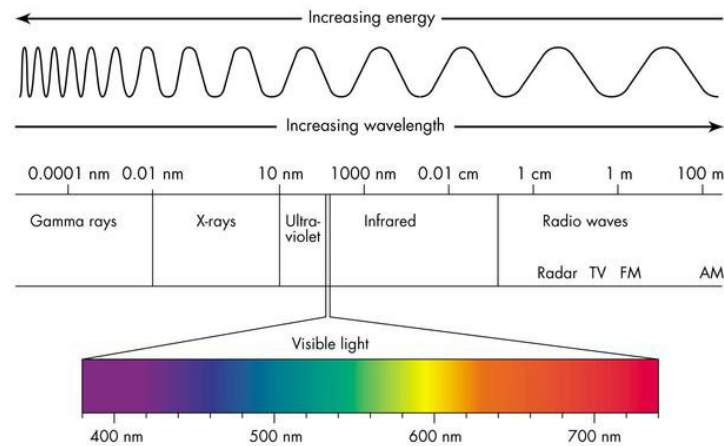
FIGURE 1.15: Electromagnetic spectrum. Figure from Wikimedia Commons.

A microfluidic chip is a set of micro-channels etched or molded into a material (glass, silicon or polymer). The micro-channels forming the microfluidic chip are connected together in order to achieve the desired features (mix, pump, sort, control bio-chemical environment). The manufacture of microfluidic chips for different applications like lab-on-chip devices is found in the literature for example at "Micro-injection moulding of Lab-on-a-chip (LOC)" by Oh et. al [26] or "Micro-injection moulding of polymer microfluidic devices" of Attia et al. [27]. The advantage of using little chips are several, among them, low fluid volumes consumption (lower reagents costs, less sample volumes for diagnostics and less waste), faster analysis and response times due to short diffusion distances, fast heating, high surface to volume ratios, better process control because of a faster system response, compactness of the systems and, hence, massive parallelization possibilities, lower fabrication costs, allowing cost-effective disposable chips, fabricated in mass production, etc.

Figure 1.16 shows a FISH (Fluorescence In Situ Hybridization) microfluidic chip, it serves as a sensitive detection microfluidic system for alzheimer's disease [28]. Specifically in this case, the channel width ranges from 10-100 µm.

– Antiwettable

On "Fabrication of Super Hydrophobic Surfaces by fs Laser Pulses" publication of Max Groenendijk [29] a method to manufacture self-cleaning surfaces with a femtosecond pulsed laser is exposed. In this work a double scale structure is used, a microstructure of pillars in the order of ten micrometers is created by scanning a raster pattern on the surface and a self organizing nanostructure is superimposed on the pillars. Both structures are created in a single processing run.

This effect is found in the nature and is called Lotus effect. Figure 1.17 shows a SEM image of the Lotus leaf surface. Indeed, research using SEM showed that even though the surfaces of the lotus leaf appear smooth with the naked eye, they exhibit microscopic roughness on different length
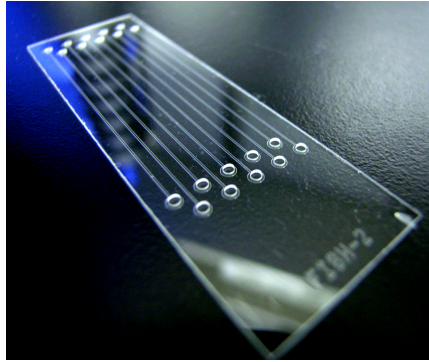
FIGURE 1.16: FISH microfluidic chip. Figure from Wikimedia Commons.

scales. These surfaces, along with the presence of hydrophobic epicuticular wax crystalloids, make the leaves superhydrophobic (Gule [1]).
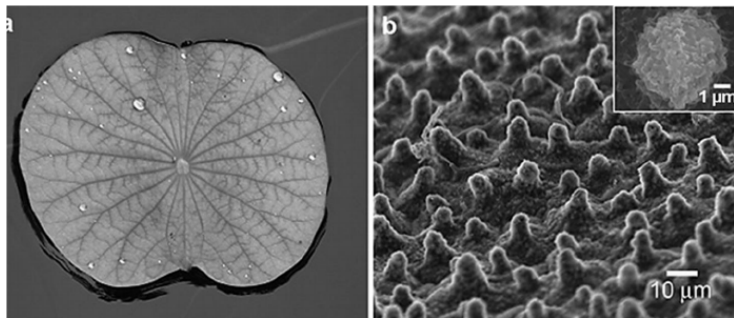
FIGURE 1.17: a) An image of Lotus leaf on the water. b) A SEM image of the Lotus leaf surface, the inset is a magnified image of the papilla structure. Figure from Gule [1].

Zhou proved in "Fabrication of high aspect ratio nanopillars and micro/nano combined structures with hydrophobic surface characteristics by injection molding" [30] that the replication of hydrophobic textures can be improved using an anti-sticking film manufactured using 1H, 1H, 2H, 2H-perfluorodecyltriethoxysilane (FAS-17) on the anodic aluminium oxide template surface.

– Antifouling

Fouling is the accumulation of unwanted material on solid surfaces, for example bacteria. Kim et al. in "Nanostructured multifunctional surface with antireflective and antimicrobial characteristics" [23] or Fadeeva et al. in "Bacterial Retention on Superhydrophobic Titanium Surfaces Fabricated by Femtosecond Laser Ablation" [31] show how a well designed nanostructure can prevent the bacterial cells attachment to the surface. Specifically, nanopilars with a period smaller than $1\mu m$ makes the bacteria uncapable to adhere.

– Modification of frictional behaviour

In microelectromechanical or nanoelectromechanical systems (MEMS and NEMS, respectively) the surface area to volume ratio increases and the body forces are irrelevant compared to the surface forces. Indeed, the surface forces may lead to permanent adhesion or large frictions between

the surfaces in contact. The use of nanorods of height 2.4 ± 0.1 μm and diameter 120 ± 20 nm for reducing the adhesive and friction forces is found to be successful as reported in "Frictional behaviors of three kinds of nanotextured surfaces" from Wu et. al [32].

– Modification of haptic properties

The haptic properties of surfaces can be changed by reducing the skin contact area, leading to a very soft feeling surface. This soft-touch effect can be used to enhance the quality/feel of consumer products. This application is found when micropillar surfaces are manufactured. Typical pillar textures use pillars with a diameter of 20-60 μm, a depth between 25 and 75 percent of the diameter, and a density of 50–2500 pillars per mm^2 [33].

A good summary of sizes, aspect ratio and depth for several applications can be found in NIL Technology website [22].

1.3 Injection moulding links nanotechnology and plastic industry

This section shows how injection molding is used as a powerful bridge between the plastics and the nanotechnology industries. From the economical point of view, injection molding has a high initial tooling and machinery cost but enables the manufacture of large series with small part costs, obtaining a fast Return of Investment when used to manufacture large series of parts. From the technical point of view, injection molding is a highly precise technique capable of building very sophisticated forms and shapes, enabling the introduction of nanostructured areas to a wide range of plastic parts with all the available thermoplastics [34].

Only when the mould nanofeatures are successfully replicated in the plastic part the MTS or the NTS lead to the specific applications. Indeed, in paper VI (Pina [4]) it is proved that light diffusion is obtained only when the nanotexture engraved in the mould is fully replicated in the plastic part. Unfortunately, when aiming to replicate in the plastic a nanocavity manufactured in the mould, the large surface-to-volume ratio of the nanoscale tends to solidify the plastic before it has reached the bottom of the nanocavity. Indeed, a situation depicted schematichally in figure 1.18 is common as reported by several researchers like Pina [5], Tofteberg [35], Rytka [36], Oh [26], etc.

The purpose of this thesis is to develop the necessary knowledge to avoid or minimize such incomplete replication. The knowledge is developed both experimentally and also by means of self-developed simulation models. Next, a brief introduction to the two approaches is done:

1.3.1 Experimental analysis

The experimental part of the thesis consists on analyzing the geometrical and process parameters that effect the replication of nanofeatures. The first step is the manufacture of nanofeatures in the mould steel, this is carried out in this thesis in three different ways:
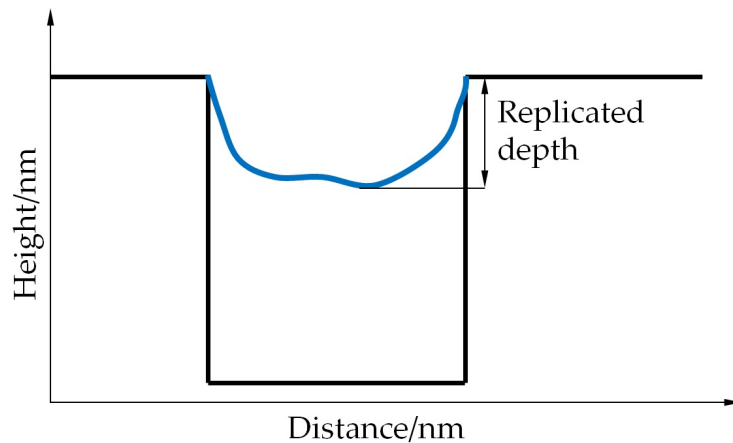
FIGURE 1.18: Schematic image of a mould cavity incomplete replication. Figure from paper V (Muntada [2]).

– Focused Ion Beam

  A FIB setup resembles a scanning electron microscope (SEM) but, instead of using a beam of electrons, a FIB setup uses a focus beam of ions. Normally, Ga^+ is used and, as it hits the surface a small amount of material is sputtered in form of secondary ions or neutral atoms. The primary beam also produces electrons. See figure 1.19 for a sketch of FIB.

  At low primary beam currents, a resolution of 5 nm is possible.
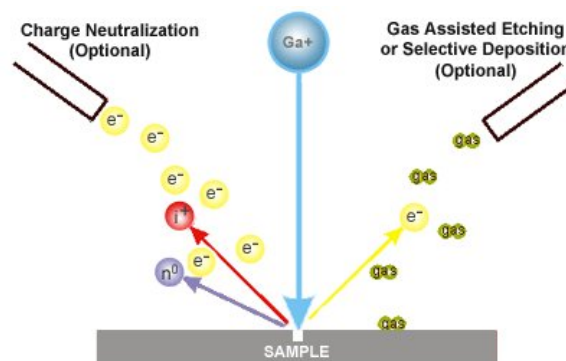
FIGURE 1.19: Principe of FIB. Figure from Wikimedia Commons.

  This method is used in paper I [5] to manufacture triangular and cross-shaped patterns of down to $2 \ \mu m$.

– Photolithography + RIE etching process

  In paper V [2], a silicon chip is manufactured with various geometries. To do so, the process depicted in figure 1.20 is pursued. In step a. the wafer comprised with silicon (substrate) and silicon oxide (oxide) is clenead in order to successfully apply the photoresist (PR) by means of a spinner. The step c. consists in aligning the photomask, which in our case was designed by us but manufactured by Photronics. In step d. the assembly is exposed to UV light in order to degradate the photoresist exposed to the UV rays. The step f. is the etching of the silicon dioxide. Finally, the remaining photoresist is removed in step g.
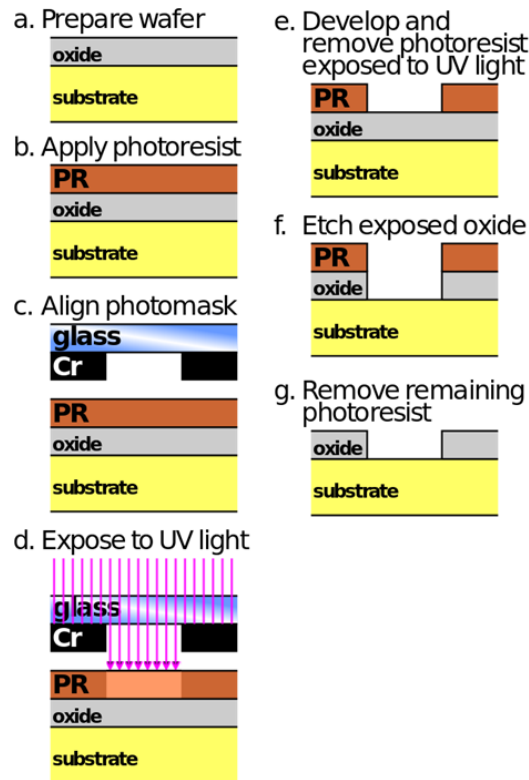
FIGURE 1.20: Photolithography + RIE etching process to manufacture
silicon chips. Figure from Wikimedia Commons.

More specifically, the RIE etching method of the step f. is a a dry etch-
ing method that uses chemically reactive plasma to remove material de-
posited on wafers. As shown in figure 1.21a, the plasma is generated
under low pressure (vacuum) by an electric field (3) created by two elec-
trodes (1 and 4). High-energy ions (2) from the plasma attack the wafer
surface (5) and react with it [37]. Because the electric field accelerates ions
toward the surface, the etching caused by these ions is much more domi-
nant than the etching of radicals or ions traveling in varied directions, so
the etching is, unlike chemical etching, anisotropic. See figure 1.21b for a
comparison between the chemical and the RIE etching.

– Laser ablation

The process of laser ablation consists on removing material from the solid
(the steel of the mould) by irradiating it with a laser beam. The laser light
excites the metal electrons which rapidly relax to lower energy states by
transferring the energy to the lattice of the material. Thereby, the mate-
rial can be melt and evaporated. This technology can be used to remove
material in a relatively controlled way. With ultrashort laser pulses the
energy is deposited in a time that is shorter than the relaxation time be-
tween the electrons and the lattice. This creates very high energy densities
and allows ablation to take place before heat conduction to the bulk mate-
rial becomes important. As a result, ultrashort laser pulses (nanosecond,
picosecond or even femtosecond laser sources) can be used to process
materials without thermally affecting the surrounding bulk material [33].

(A) RIE sketch. Figure from Wikimedia Commons.

(B) Comparison between chemical and RIE etching. Figure from Wikimedia Commons.
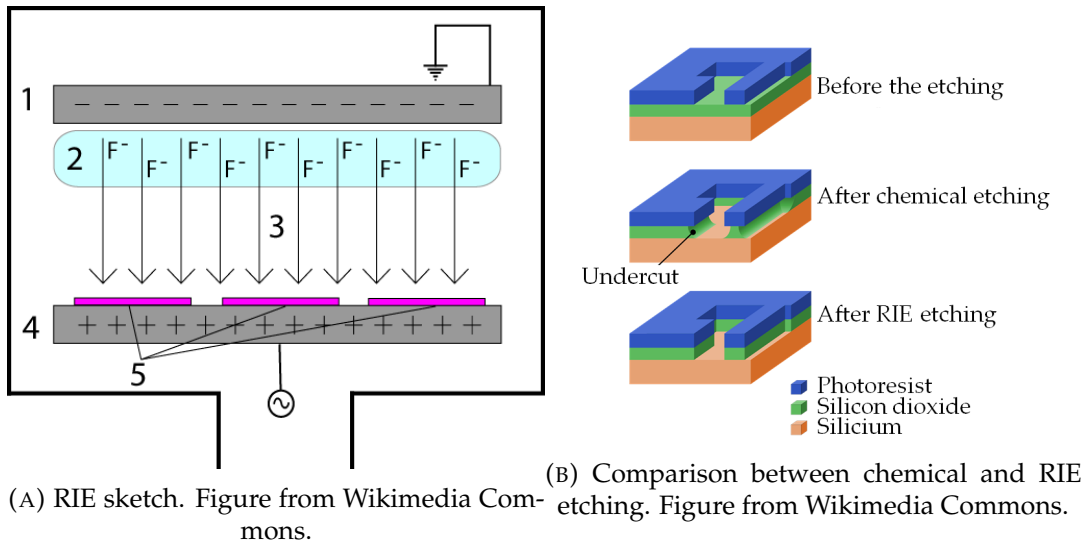
FIGURE 1.21: RIE sketches.

See figure 1.22 for three sketches showing the decreasing thermal affectation of continuous wave lasers, nanosecond lasers and pico/femtosecond lasers.

At paper VI (Pina [4]), SEAT and IQS (Ramon Llull University) joined efforts and developed an industrial application consisting in the manufacture of surfaces with optical applications. The NTS that make possible such applications were engraved in the laser mould with nano and femtosecond lasers.
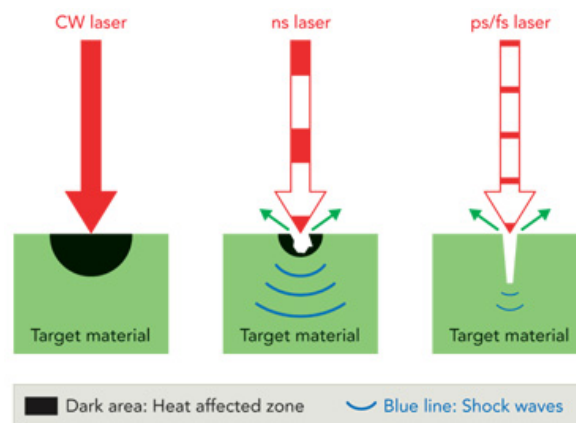
FIGURE 1.22: Comparison of thermal affectation of continuous wave, nanosecond and pico/femtosecond lasers. Figure from [3].

Independently from the manufacturing method, it is important to consider the large number of nanofeatures necessary to fill a given area. For example, filling a $10\text{mm} \cdot 10\text{mm}$ surface with $0.1\mu\text{m}$ diameter nanopillars with a separation between nanopillars of $0.1\mu\text{m}$ leads to a surface with $2.5 \cdot 10^9$ nanopillars. This makes injection moulding manufacturing technique one of the most cost-effective approaches, indeed, the large cost of manufacturing such big amount of nanofeatures will be amortized with the large number of plastic parts that the mould will produce.

(A) Sketch of an AFM. Figure from Wikimedia Commons.

(B) AFM images of the transferred patterns placed at the centre of the mould (G2) and corresponding cross sections are depicted. Figure from paper I (Pina [5])
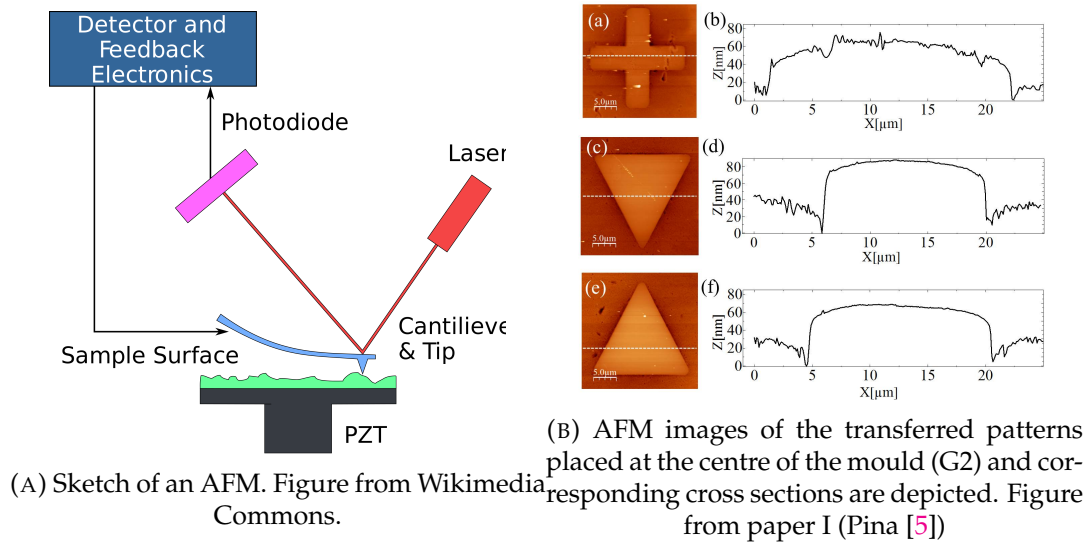
FIGURE 1.23: AFM sketch and measurement example.

Once the nanofeatures are manufactured in the mould, the plastic injection can be pursued. Several injection parameters like material drying conditions, mould temperature, melt temperature, filling time, demoulding conditions, packing pressure and others need to be correctly tuned in order to assure the nanofeature replication. In paper IV (Pina [8]) and V ([2]) a detailed Design of Experiments is pursued in order to quantify the effect of these parameters in the replication. Such quantification needs specific measurement methods to measure the resulting nanofeatures, in this thesis, three microscopy methods and a roughness tester has been used:

– Atomic Force Microscope (AFM)

   An Atomic Force Microscope is a type of scanning probe microscopy (SPM), what means that the images of surfaces are formed using a physical probe that scans the specimen (see figure 1.23a for an sketch of an AFM). The resolution is on the order of fractions of a nanometer, more than 1000 times better than the optical diffraction limit. Despite its advantages, the measured part must be flat. AFM is used in paper I (Pina [5]) to measure the replication of the cavities manufactured in the mould, see figure 1.23 for an example.

– Scanning Electron Microscope (SEM)

   A scanning electron microscope (SEM) is a type of electron microscope that produces images of a sample by scanning it with a focused beam of electrons. The electrons interact with atoms in the sample, producing various signals that contain information about the sample's surface topography and composition. The electron beam is generally scanned in a raster scan pattern, and the beam's position is combined with the detected signal to produce an image. SEM can achieve better resolution than 1 nanometer. See figure 1.24a for a sketch of the SEM working principle and figure 3.4a for a measurement example.

– Optical microscopy (confocal and focus variation)

(A) Sketch of a SEM. Figure from Wikimedia Commons.

(B) SEM images of the FIB patterns on mould. Figure from paper I (Pina [5])
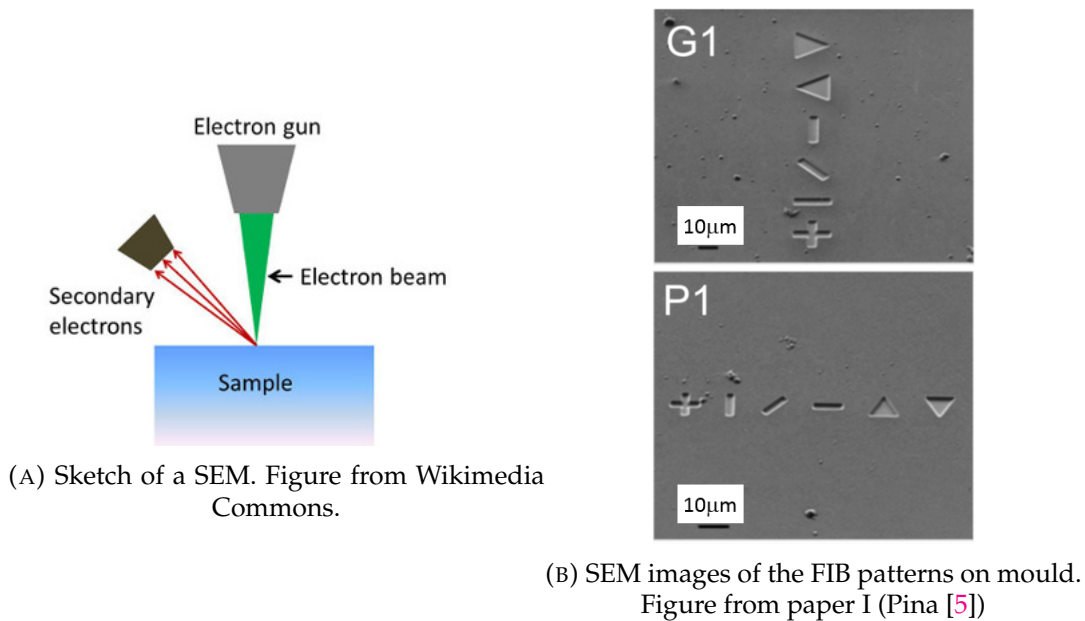
FIGURE 1.24: AFM sketch and measurement example.

Optical microscopes are non-contact 3D surface measurement methods, they capture 3D spatial coordinates of points on a surface using a non-destructive (unlike SEM) and non-contact optical technique (unlike AFM). The most common optical techniques available are confocal, interferometry and focus variation. Specifically in paper VI (Pina [4]), a Sensofar S Lynx microscope is used. It incorporates a confocal (best for surfaces with high slope) and focus variation (measure shape in mere seconds) technologies in a single sensor head is used. See figure 1.25 for an example.
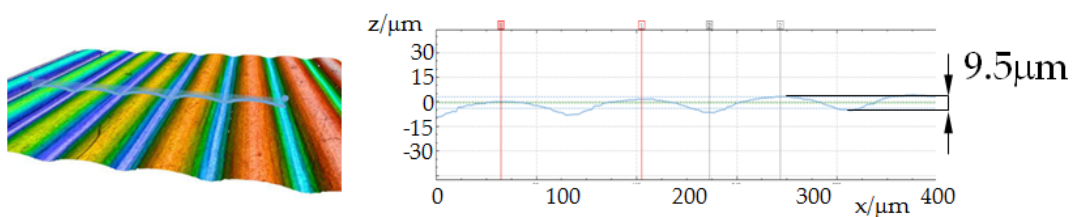
FIGURE 1.25: Confocal image of the plastic part with light heterogene diffusion. Figure from paper VI (Pina [4]).

– Surface roughness tester

A roughness tester is used in paper VI (Pina [4]) to measure the roughness of the textures with optical applications. Roughness testers have a tip that goes through the surface a given distance. When aiming to measure the roughness of a surface it is important to be aware that the raw profile is the composition of the primary profile, form, waviness and roughness, see figure 1.26. Hence, measuring the roughness of a surface that has a waviness profile is not straight forward and must be done properly, typically, the cut off value of the roughness tester is set to a smaller value than the waviness profile period, serving thus as a filter of the waviness frequency.
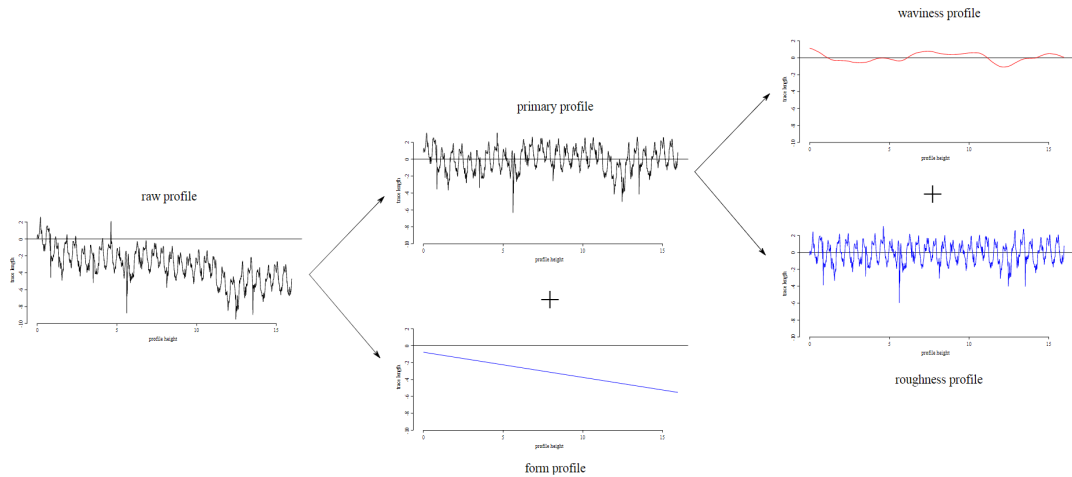
FIGURE 1.26: Illustration showing how the raw profile from a surface finish trace is decomposed into a primary profile, form, waviness and roughness. Figure from Wikimedia Commons.

A common difficulty when measuring small nanofeatures in large plastic parts is finding them in the macro part. For simplicity, it is useful to manufacture large marks that help finding the nanofeatures.

1.3.2 Simulation analysis

The theoretical part of this work consists on developing a computational model able to foresee the replication of nanocavities as a function of process parameters (polymer and mould temperature, filling time, maximum inlet pressure, demoulding conditions, etc.), geometrical parameters (position of the nanostructures in the macropart and its geometry) and the molecular structure of the polymer. With this purpose, two simulation models have been developed taking as a basis two simulation procedures: Computational Fluid Dynamics and Molecular Dynamics.

Either with CFD or MD approaches, the first problem that arises is the computational limitation. From the Computational Fluid Dynamics point of view it is impossible to mesh the whole part with a nanoscale mesh, indeed, it is proved in paper I (Pina [5]) that performing a simulation of a $(50 \cdot 50 \cdot 3)$ mm^3 part would lead to a calculation time of $1.9 \cdot 10^{22}$ years. The refining approach is also proved to lead to unphysical results when cm-sized and nm-sized mesh elements are combined. From the Molecular Dynamics point of view, it is obviously impossible to perform the simulation of the vast number of molecules that fills a macro scale part. This is solved both for CFD and MD with the submodeling approach, it consists of performing first a macro simulation with a commercial software (for example Solidworks Plastics) and using the results of this simulation as BC of a second nanoscale simulation, performed either with CFD or MD.

Next, the CFD and MD approaches are explained:
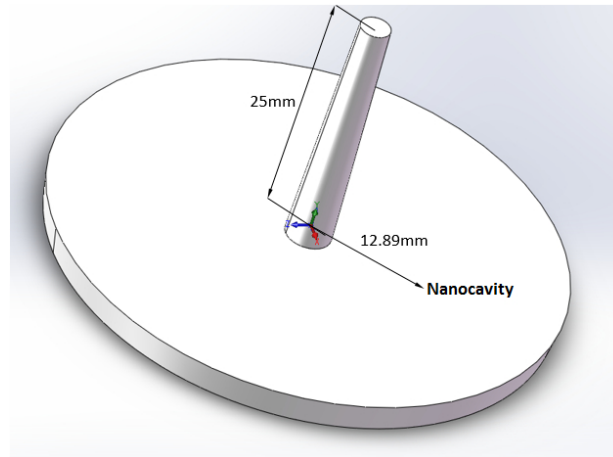
(A) CAD model used for the macro simulation first stage. Figure from paper I (Pina [5]).
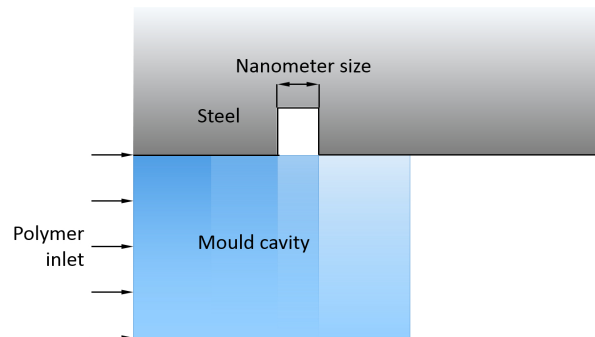
(B) Macro simulation, the graduates tones in blue indicate the polymer advance. It is considered that the fluid goes through the cavity without noticing its presence. Figure from paper I (Pina [5]).

FIGURE 1.27: First and second steps of the submodeling approach.

Computational Fluid Dynamics

Computational Fluid Dynamics is a branch of fluid dynamics used in this thesis to perform simulations of nanocavities replication in papers I (Pina [5]), II (Pina [38]) and V ([2]). The mathematical approach is the Finite Volume Method, in which the solution domain is subdivided into a finite number of small control volumes. The conservation equations of mass, momentum and energy are discretized and solved for each cell at each time step.

The submodeling approach consists in performing first a filling simulation at the whole geometry with a commercial software (see figure 1.27a), without even considering the nanostructures. In fact, it is supposed that the macro polymer flow is not affected by the presence of the nanostructure due to its small size (see figure 1.27b).

Second, the nanoscale simulation is performed, where the polymer temperature and the pressure profile are extracted from the macrosimulation results, see figure 1.28.
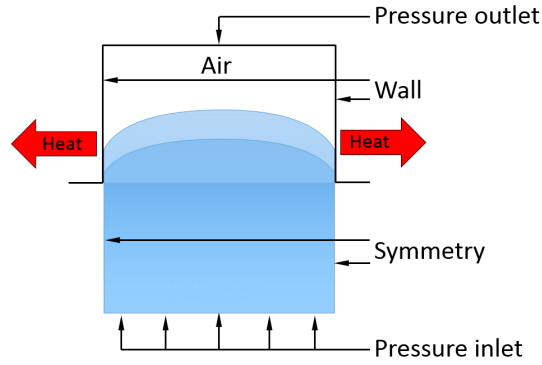
FIGURE 1.28: Nano simulation, the graduated tones in blue indicate the polymer advancing into the nanocavity until it reaches the glass transition temperature. The boundary conditions are indicated. Figure from paper I (Pina [5]).

The nanosimulation can be expanded to the three dimensions and, then, the effect of the nanocavity geometry in the replication can be studied. In paper II (Pina [7]) it is studied when 3D simulations are necessary to obtain accurate results even at the expense of a higher computational cost and how it is possible to foresee the final shape of the polymer.

This model can be considered a function with the variables of equation 1.1.

$$
\begin{bmatrix}
\text{Replicated depth} \\
\text{Time until NFT} \\
\text{polymer final shape}
\end{bmatrix}
= f
\begin{bmatrix}
\text{polymer physical properties} \\
\text{polymer temperature} \\
\text{polymer rheology} \\
\text{mould temperature} \\
\text{cavity geometry} \\
\text{filling time} \\
\text{maximum inlet pressure}
\end{bmatrix}
\tag{1.1}
$$

Molecular Dynamics

Molecular Dynamics is an N-body simulation to study the physical movements of atoms and molecules. Molecular Dynamics is used in this thesis with two purposes: (i) simulating the filling of cavities with dimensions that make the continuum approach of the CFD not valid and (ii) studying the effect of the polymer molecular structure in the replication of nanocavities.

Figure 1.29 depicts qualitatively that the application range of MD covers all the range of geometries, with the only limitation of the computational resources needed. On the other hand, CFD approach looses precision at around 100 nm, when continuum approach is not valid anymore.

Unlike CFD, Molecular Dynamics does not mesh the part because the equations are solved for each atom and not for each cell. However, the submodeling approach is also used in order to avoid the computational resources that would be necessary to calculate the filling of the macro part with an atomistic detail. Like in the previous section, a first macro simulation is carried out using Solidworks Plastics. Next, the MD simulation is pursued using as input data the the results of the first simulation. Figure 1.30 depicts the flow of information between the CFD macrosimulation and the MD nanosimulation.
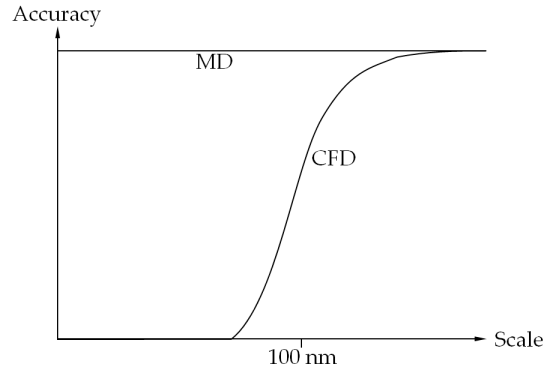
FIGURE 1.29: Qualitative plot showing the scales at which MD and CFD approaches are accurate. Own source image.
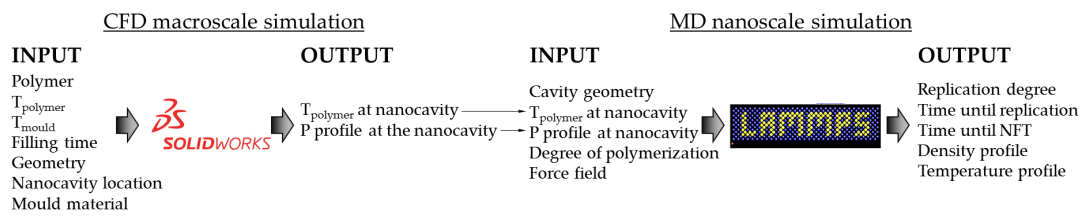
FIGURE 1.30: Submodeling approach for coupling CFD macrosimulation with MD nanosimulation. Figure from paper III (Pina [6]).

The MD nanosimulation comprises three different steps as in detail exposed in paper III (Pina [6]):

1. Force field definition.

   The force field used to calculate the potential energy of a system of atoms is defined. In paper III (Pina [6]), the generic DREIDING force field is used. A force field has 2 parts: the formulas that define it (see equation 1.2) and the coefficients used for the studied system. The main equation is:

   $$E = E_{bond} + E_{angle} + E_{torsion} + E_{vdw} =$$
   $$= k_b(r - r_0)^2 + k_a(\theta - \theta_0)^2 + k_t(1 + cos(n\phi - \phi_0)) + 4\epsilon \left(\left(\frac{\sigma}{r} \right)^{12} - \left(\frac{\sigma}{r} \right)^6 \right)$$
   $$(1.2)$$

   Where E_{bond}, E_{angle}, $E_{torsion}$ and E_{vdw} energies are defined below:

   – E_{bond} is the energy of a bond connecting two atoms. The energy of a bond is minimum at the equilibrium bond radius. If the bond is then compressed the electron clouds of the two atoms forming it will gradually overlap, leading to a rapid increase in energy. If the bond is stretched beyond equilibrium the energy starts to increase. Eventually, however, the bond disassociates. k_b is the constant of bond stretching potential, r is the bond radius and r_0 the equilibrium bond radius.

   – E_{angle} is the energy needed to distort the angle formed when three atoms are connected with two bonds. This energy is much lower

          than the one needed to distort a bond, so consequently bond angle bending force constants tend to be proportionally smaller than those for bond stretching. k_a is the angular bending potential, θ is the bond angle and θ_0 the equilibrium bond angle.

       – $E_{torsion}$ is the energy needed to distort the middle bond formed by four atoms, this energy is periodic through a 360° rotation and, hence, it is defined with a cos function. k_t is the torsion potential, ϕ is the dihedral angle and ϕ_0 the equilibrium dihedral angle.

       – E_{vdw} is a non-bonded interaction that includes attraction and repulsions between atoms, molecules, and surfaces, as well as other intermolecular forces. They differ from covalent and ionic bonding in that they are caused by correlations in the fluctuating polarizations of nearby particles. This energy is modeled with the Lennard-Jones potential equation, where ϵ is the depth of the potential well and σ is the finite distance at which the inter-particle potential is zero.

All the coefficients are obtained from the original Mayo publication of 1990 (Mayo [39]) entitled "DREIDING: a generic force field for molecular simulations".

2. Model construction

An initial configuration of polymer chains with a given degree of polymerization is created. This configuration must approximately represent the system's overall structure and, in order to avoid blowing up the simulation due to large Van der Waals repulsive interactions, all the atoms of the initial configuration must keep safe pairwise distances. This is called a packing problem and is pursued trough the combination of different softwares like Polymer Modeler, Packmol and VMD with TopoTools plugin.

3. Simulation

First, the initial configuration is loaded, the mould atoms added and the geometry shrinked until the target geometry. Second, a minimum on the potential energy surface is found with increasing pair coefficients. Third, the polymer is equilibrated to the target density. Finally, the production run is pursued until the polymer reaches the NFT.

In figure 1.31 different snapshots are depicted from the beginning of the replication until the NFT. It is shown how the replication is studied in atomistic detail, enabling the possibility to track the position of each atom of the polymer chains. The fact that the polymer is modeled not through bulk parameters like density, heat capacity or viscosity but through the defined force field makes the study of the polymer molecular structure effect in the replication possible. In paper IV (Pina [8]) the effect of polymer chain length and tacticity are successfully quantified.

To sum up, the developed algorithm that links a macro CFD simulation with a nano MD simulation can be understood as a function with the inputs and outputs shown in equation 1.3.

0ns   0.005ns   0.015ns   0.1ns   0.49ns

2.4nm
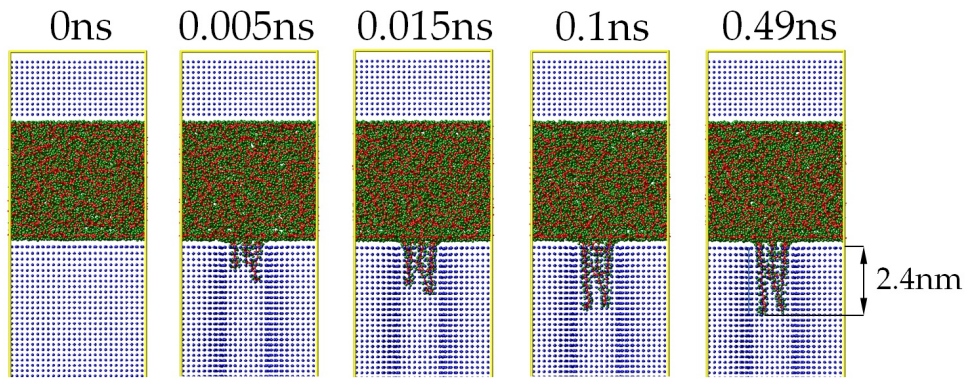
FIGURE 1.31: Evolution of cavity replication for the simulation with entrance area $1.6 \cdot 1.6 \ \mathrm{nm}^2$. Figure from paper III (Pina [6]).

$$
\begin{bmatrix}
\text{Replicated depth} \\
\text{Time until NFT} \\
\text{Density} \\
\text{atoms position}
\end{bmatrix}
= f
\begin{bmatrix}
\text{polymer molecular geometry} \\
\text{polymer temperature} \\
\text{mould temperature} \\
\text{cavity geometry} \\
\text{force field} \\
\text{filling time} \\
\text{maximum inlet pressure}
\end{bmatrix}
\qquad (1.3)
$$

Chapter 2

Publications derived from this thesis

The research pursued during the PhD has led to the publication of five publications in peerreviewed journals, one publication currently under review (paper V) and 6 communications in international congresses.

A summary of each paper along with the Jordi Pina specific contribution to the publication is detailed below:

– Paper I

Pina-Estany, J., Colominas, C., Fraxedas, J., Llobet, J., Perez-Murano, F., Puigoriol-Forcada, J. M., ... Garcia-Granada, A. A. (2017). A statistical analysis of nanocavities replication applied to injection moulding. International Communications in Heat and Mass Transfer, 81, 131-140.

In this paper, the submodeling approach is first exposed and used to couple a CFD macrosimulation with a CFD micro/nanosimulation, the main affecting factors are statistically studied (melt and mould temperature, filling time and cavity geometry) but only for 2D geometries. It is experimentally proven that the polymer goes initially through the nanocavity without noticing its presence and gets into a second stage.

Jordi Pina developed the submodeling approach presented in this work and designed and performed the simulations necessary for the presented Design of Experiments. The experimental trials were prepared by all the authors and were pursued in CSIC. The submission and the following communication with the journal until the publication was pursued by Jordi Pina.

– Paper II

Pina-Estany, J., García-Granada, A. A. (2017). 3D Simulation of Nanostructures Replication via Injection Molding. International Polymer Processing, 32(4), 483-488.

The submodeling approach presented in paper I is expanded to 3D and is proved that 3D simulations are necessary when the cavities have a relationship between length and width smaller than 4 or it is intended to know the final shape of the polymer. For other geometries, 2D simulations are preferable because the computational resources and the computation time are substantially lower.

Jordi Pina expanded the submodeling approach presented in paper I to the 3D and pursued all the simulations that leaded to this work. The

submission and the following communication with the journal until the publication was pursued by Jordi Pina.

– Paper III

Pina-Estany, J., García-Granada, A. A. (2017). Molecular dynamics simulation method applied to nanocavities replication via injection moulding. International Communications in Heat and Mass Transfer, 87, 1-5.

Even though in paper I and II the simulation of microscale geometries of down to $100 \cdot 50 \text{nm}^2$ have been successfully simulated, such dimensions are already at the boundary of the CFD capabilities. In this paper, the continuum hypothesis limitation of CFD is overcome and the submodeling approach is expanded in order to make a coupling of a macro CFD simulation with a nanoscale Molecular Dynamics simulation possible. Specifically, the effect of the entrance area in the replication is studied with atomistic detail.

Jordi Pina developed the submodeling approach based in Molecular Dynamics and studied the replication of nanocavities with it. The submission and the following communication with the journal until the publication was pursued by Jordi Pina.

– Paper IV

Pina-Estany, J., García-Granada, A. A. (2018). Computational analysis of polymer molecular structure effect on nanocavities replication via injection moulding. Afinidad, 75(581).

In this publication, the model developed in paper III is used to study the effect of the molecular structure in the replication of nanocavities, more specifically, the degree of polymerization of PE and the tacticity of PS are analysed and found to be affecting factors.

Jordi Pina applied in this publication the mathematical model developed in paper III and pursued the simulations that leaded to the quantification of the tacticity and the degree of polymerization in the replication of nanocavities. The submission and the following communication with the journal until the publication was pursued by Jordi Pina.

– Paper V (under review)

Olga Muntada-Lopez, **Jordi Pina-Estany**, Carles Colominas, Jordi Fraxedas, Francesc Perez-Murano , Andres Garcia-Granada (2018). Replication of nanoscale surface gratings via injection molding. Under review.

Even though this publication has not been accepted at the date of the thesis delivery, it is included in this thesis because its results are part of the pursued research. This publication is essentially an experimental paper developed with CSIC and Flubetech in which several injections are pursued in moulds with nanostructured gratings in order to study the effect of process and geometric factors. The highlight of this paper is that it studies the replication of consecutive nanocavities, whereas the papers I to IV are focused in the replication of single nanocavities. When the replication of consecutive nanocavities is studied, it is found that the separation between them is a factor with a large effect in the replication, this is further analyzed by means of CFD simulation. In addition, a previously not reported sinking effect in the nanostructured area and a shrinking of the pattern period were characterized and simulated.

Jordi Pina participated in the design of the work, specifically in the decision of what geometries would be created by means of photolithograpy

and Reactive Ion Etching and in the preparation of the Design of Experiments. The simulations with different w values were performed by Jordi Pina and this part of the publication was written by him.

– Paper VI

Pina-Estany, J., García-Granada, A. A., Corull-Massana, E. (2018). Injection moulding of plastic parts with laser textured surfaces with optical applications. Optical Materials, 79, 372-380.

Finally, in paper VI, IQS (Ramon Llull University) and SEAT lighting department joined efforts and studied together the use of nanotextures to obtain optical application. For this publication, moulds are laser-textured and plastic is injected in moulds with induction heating warming method. Jordi Pina leaded the obtaining of plastic parts with nanotexturised parts, comprising it the manufacture, laser texturised and injections with Heat-Cool warming method. Once the parts were available, Jordi Pina took personally the necessary measures with the luminance camera to reach the conclusions stated in the paper. The submission and the following communication with the journal until the publication was pursued by Jordi Pina.

– Paper VII (future work)

Paper VII is not included in the thesis but, since it is in process at the moment of the thesis defense, some words about the further work are included here. Indeed, paper VII will be a zoom in the effect of mould temperature in the replication of laser-manufactured textures. In paper VI two injection conditions were analyzed: 55°C with conventional injection and 115°C with induction heating injection. In the upcoming paper VII, the efficiency and the homogeneity will be studied through a range of temperatures from 50°C to 90°C with conventional injection and from 90°C to 150°C with induction heating injection.

The six communications in international congresses are:

– Congress communication I

J.Pina-Estany; J.Fraxedas; F.Perez-Murano; C.Colominas; J.M.Puigoriol-Forcada; A.A.Garcia-Granada "Simulation of plastic injection for nanostructure pattern replication" PRN 2015 Poster Vol. — N.— Pag: — Year: 18-19 May 2015 Place of publication: DTU Copenhagen, DK

– Congress communication II

J.Pina-Estany; J.Fraxedas; F.Perez-Murano; C.Colominas; J.M.Puigoriol-Forcada; A.A.Garcia-Granada "Simulation of plastic injection for nanostructure pattern replication" MNC 2015 Poster Vol. — N.— Pag: — Year: 8-9 December 2015 Place of publication: Amsterdam, NL

– Congress communication III

J.Pina-Estany; J.Fraxedas; F.Perez-Murano; C.Colominas; J.M.Puigoriol-Forcada; A.A.Garcia-Granada "Simulation of plastic injection for nano roughness replication" ICME 2016 Poster Vol. — N.— Pag: — Year: 12-15 April 2016 Place of publication: Barcelona, ES

– Congress communication IV

J.Pina-Estany; J.Fraxedas; F.Perez-Murano; C.Colominas; J.M.Puigoriol-Forcada; A.A.Garcia-Granada "Fluent solver expanded to the nano-world"

PRN 2016 Poster Vol. — N.— Pag: — Year: 19-20 May 2016 Place of publication: FHNW University of Applied Sciences and Arts Northwestern Switzerland, Widisch , CH

– Congress communication V

   J.Pina-Estany; J.Fraxedas; F.Perez-Murano; C.Colominas; J.M.Puigoriol-Forcada; A.A.Garcia-Granada "Submodelling simulation of plastic injection for nano roughness replication" Industrial Technologies 2016 Poster Vol. — N.— Pag: — Year: 22-24 June 2016 Place of publication: Amsterdam, NL

– Congress communication VI

   O.Muntada-Lopez; **J.Pina-Estany**; J.Fraxedas; F.Perez-Murano; C.Colominas; A.A.Garcia-Granada "Simulations and testing of polymer replication on nanoscale" PRN 2017 Poster Vol. — N.— Pag: — Year: 8-9 May 2017 Place of publication: Fraunhofer IPT / WZL Aachen, DE

2.1 Paper I: A statistical analysis of nanocavities replication applied to injection moulding

The purpose of this paper is to investigate both theoretically and experimentally how nanocavities are replicated in the injection moulding manufacturing process. The objective is to obtain a methodology for efficiently replicate nanocavities.

From the theoretical point of view, simulations are carried out using a submodeling approach combining Solidworks Plastics for a first macrosimulation and Fluent solver for a subsequent nanosimulation. The effect of the four main factors (melt temperature, mould temperature, filling time and cavity geometry) are quantified using an statistical 24 factorial experiment. It is found that the main effects are the cavity length, the mould temperature and the polymer temperature, with standardized effects of 5, 3 and 2.6, respectively. Filling time has a negative 1.3 standardized effect. From the experimental point of view, Focused Ion Beam technique is used for mechanizing nanocavities in a steel mould. The replication achieved in polycarbonate injection is quantified using an Atomic Force Microscope. It is observed how both the geometry and the position of the cavities in the mould affect its replication.

2.2   Paper II: 3D simulation of nanostructures replication via injection moulding

The purpose of this paper is to shed light on how and when 3D simulations are preferable over 2D simulations in order to predict the replicated height of nanocavities via plastic injection moulding. Simulations are necessary since not all the cavity is copied depending on geometrical and injection conditions. A 3D simulation is preferable over a 2D simulation in two cases: (i) when the heat transfer through the walls parallel to the simulated domain is not negligible and (ii) when the polymer final shape is relevant. This work explains when 2D simulations like the more commonly found in the literature are not enough to obtain reliable results and how to obtain such results by means of a 3D simulation.

https://doi.org/10.3139/217.3383

2.3 Paper III: Molecular dynamics simulation method applied to nanocavities replication via injection moulding

Injection moulding is a promising manufacturing process to obtain cost-effective plastic parts with nanostructured surfaces. However, nanocavities replication is not a straightforward method because the large heat transfer that takes place at the nanoscale tends to solidify the polymer before it has replicated all the cavity. This behaviour has been studied by different authors by means of Computational Fluid Dynamics simulations, in this way, process parameters (mould and melt temperatures, filling time, injection pressure limit, holding time, etc.) and geometric parameters (cavity geometry, cavities location in the mould, etc.) factors have been quantified. However, such investigations have found a roadblock when aiming to evaluate the replication of nanocavities with dimensions smaller than 100nm, the reason is that the continuum hypothesis in which Computational Fluid Dynamics is based is not valid anymore. The purpose of this work is to overcome the scale limitation of Computational Fluid Dynamics and expose a Molecular Dynamics based algorithm to foresee the replication of nanocavities.

2.4 Paper IV: Computational analysis of polymer molecular structure effect on nanocavities replication via injection moulding

The purpose of this work is to study how the molecular structure of a polymer affects the replication of nanocavities when injection moulding manufacturing process is used. Even though the process and geometrical factors that affect the replication of nanocavities have been studied by several authors, the effect of the polymer molecular structure on the injection result remains so far unstudied.

In order to study through simulation the molecular structure influence, Computational Fluid Dynamics methods are not valid because they consider the matter a continuum. This limitation is overcome by means of Molecular Dynamics simulation method, within each atom movement is tracked in a sort of n-body problem.

With a self-made model, the effect of degree of polymerization and tacticity are successfully quantified in the replication of nanocavities of down to $2 \cdot 2 \mathrm{nm}^2$. It is concluded that the degree of polymerization has a negative effect on the nanocavity replication due to the easier entanglement of longer polymer chains. Concerning to the tacticity effect, it is found out that syndiotactic polystyrene replicates less than atactic or isotactic polystyrenes because of the larger entanglement of the phenyl groups when in alternate positions along the chain.

https://www.raco.cat/index.php/afinidad/article/view/335956

Computational analysis of polymer molecular structure effect on nanocavities replication via injection moulding

J. Pina-Estany*[1] and A.A. García-Granada[1]

[1]IQS-Universitat Ramon Llull, Via Augusta, 390. 08017, Barcelona (Spain)

Análisis computacional del efecto de la estructura molecular en la copia de nanocavidades mediante inyección de plástico

Anàlisi computacional de l'efecte de l'estructura molecular en la còpia de nanocavitats mitjançant la injecció de plàstic

SUMMARY

The purpose of this work is to study how the molecular structure of a polymer affects the replication of nanocavities when injection moulding manufacturing process is used. Even though the process and geometrical factors that affect the replication of nanocavities have been studied by several authors, the effect of the polymer molecular structure on the injection result is less studied.

In order to study through simulation the molecular structure influence, Computational Fluid Dynamics methods are not valid because they consider the matter a continuum. This limitation is overcome by means of Molecular Dynamics simulation method, in which each atom movement is tracked in a sort of n-body problem.

With a self-made model, the effect of degree of polymerization and tacticity are successfully quantified in the replication of nanocavities of down to $2 \cdot 2 nm^2$. It is concluded that the degree of polymerization has a negative effect on the nanocavity replication due to the easier entanglement of longer polymer chains. Concerning the tacticity effect, it is found out that syndiotactic polystyrene replicates less than atactic or isotactic polystyrenes because of the larger entanglement of the phenyl groups when in alternate positions along the chain.

Keywords: Computational Fluid Dynamics; injection moulding; Molecular Dynamics; nanoscale simulation; submodeling.

SUMARIO

El objetivo de este trabajo es estudiar cómo la estructura molecular de un polímero afecta la copia de nanocavidades cuando se utiliza inyección de plástico. Si bien distintos autores han estudiado los factores geométricos y de proceso que afectan a la replicación, el efecto de la estructura molecular del polímero en el resultado de la inyección no se ha analizado tan en detalle.

Con el objetivo de estudiar el efecto de la estructura molecular mediante simulación, la dinámica de fluidos computacional no es válida porque considera la materia un continuo. Esta limitación se supera usando la dinámica molecular, de forma que el movimiento de cada átomo se simula como si fuese un problema de n-sólidos.

Mediante un modelo propio, el efecto del grado de polimerización y la tacticidad se cuantifican con éxito en nanocavidades de hasta $2 \cdot 2 nm^2$. Se concluye que el grado de polimerización tiene un efecto negativo en la copia de nanocavidades debido al menor entrelazamiento de las largas cadenas de polímero. Referente a la tacticidad, se prueba que el poliestireno sindiotáctico copia en menor cantidad las nanocavidades que el atáctico o el isotáctico, debido al mayor entrelazamiento de los grupos fenilo cuando se ubican en posiciones alternadas de la cadena.

Palabras clave: Dinámica de fluidos computacional; inyección de plástico; dinámica molecular; simulación a escala nanométrica; submodelado.

SUMARI

L'objectiu del treball és estudiar com l'estructura molecular d'un polímer afecta la còpia de nanocavi-

*Corresponding author: jordipinae@iqs.url.edu

tats quan s'utilitza la injecció de plàstic. Si bé diversos autors han estudiat els factors geomètrics i de procés que afecten la replicació, l'efecte de l'estructura molecular del polímer en el resultat de la injecció no s'ha analitzat tan en detall.

Amb l'objectiu d'estudiar l'efecte de l'estructura molecular mitjançant una simulació, la dinàmica de fluids computacional no és vàlida perquè considera la matèria un continu. Aquesta limitació se supera fent ús de la dinàmica molecular, de manera que el moviment de cada àtom se simula com si fos un problema de n-sòlids.

Mitjançant un model propi, l'efecte del grau de polimerització i la tacticitat es quantifiquen amb èxit en nanocavitats de fins a 2·2nm^2. Es conclou que el grau de polimerització té un efecte negatiu en la còpia de nanocavitats a causa d'un menor entrellaçament de les llargues cadenes de polímer. Pel que fa a la tacticitat, es demostra que el poliestirè sindiotàctic copia menys les nanocavitats que l'atàctic o l'isotàctic a causa d'un menor entrellaçament dels grups fenil quan s'ubiquen en posicions alternades de la cadena.

Paraules clau: Dinàmica de fluids computacional; injecció de plàstic; dinàmica molecular; simulació a escala nanomètrica; submodelat.

1. INTRODUCTION

Nanostructured surfaces are used for different applications such as lab-on-chips devices[1], antimicrobial surfaces[2], surfaces with self-cleaning capabilities[3], water purification[4], optical applications to achieve antireflection[5] or transmission enhancements[6], etc. The vast majority of these parts are made of plastic and, from the different manufacturing processes, injection plastic is the most suitable one because of its low production costs. However, replicating a nanostructure is not straightforward because the large surface-area-to-volume ratio of the nanoscale tends to solidify the polymer before it has reached the bottom of the nanocavities, see figure 1 for an schematic figure of an incomplete replication.

In order to understand how the replication can be successfully achieved, several authors have studied how process and geometrical parameters can be tuned in order to improve the replication. The current available know-how was developed both experimentally[7-11] and also via simulation[12-16]. These works show which factors have a positive effect (cavity length, mould temperature, melt temperature, etc.) and which have a negative effect (filling time, for example). However,
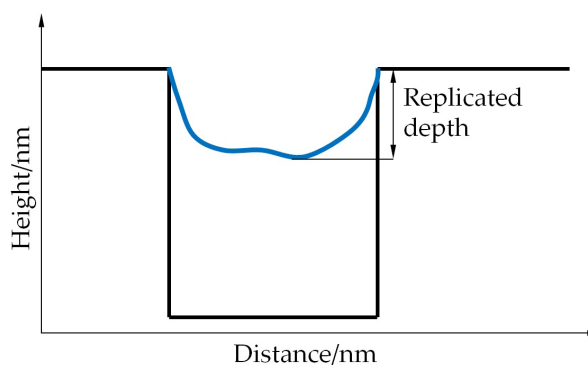
Figure 1: *Schematic image of an incomplete cavity replication.*

these works simulate the polymer behaviour with Computational Fluid Dynamics approaches, which are not valid for dimensions smaller than 100nm because they consider the matter a continuum. Besides, they cannot consider the molecular structure because the fluid is modeled through bulk parameters (density, viscosity, heat capacity, etc.). In this work, the Molecular Dynamics algorithm published in "Molecular dynamics simulation method applied to nanocavities replication via injection moulding"[17] is used to study the effect of the degree of polymerization and the tacticity in the replication of cavities with dimensions smaller than 100nm.

The use of Molecular Dynamics simulation method is growing along with the increase of the computational resources, indeed, MD is used to study different topics such as the heat transfer at the microscale[18], the flow of liquids at the nanoscale[19], the polymer crystallization from the melt[20], the simulation of thread break-up and formation of droplets in nanoejection system[21], etc. Related specifically to the replication of nanocavities via injection molding, Feng studies in "Molecular dynamics simulation of injection of polyethylene fluid in a variable cross-section nano-channel"[22] the effects of the nano-channel cross section and the external forces. Zhou analyzes in "Molecular dynamics study on polymer filling into nano-cavity by injection molding"[23] the effect of molecular weight and cavity size.

2. METHODS

Since it is computationally unaffordable to carry out a Molecular Dynamics simulation of a macro part, the submodeling approach is used to reduce the computational requirements. It consists in coupling a first macro-CFD simulation with a subsequent nano-MD simulation. The two simulation steps are summarized here under:

Macro-CFD simulation

Using SolidWorks Plastic, an injection plastic simulation is performed in the geometry of figure 2 with 3 mm thickness.

Polymer inlet

25 mm

x

Nanostructure

50 mm

Figure 2: *Macro geometry used in the macro-CFD simulation.*
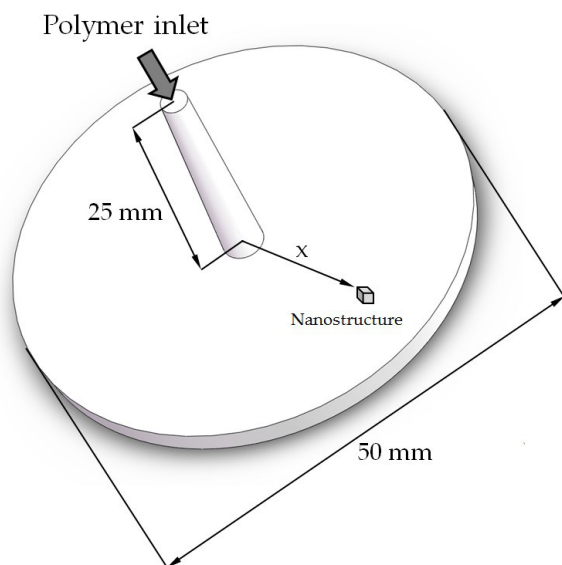
The pressure profile is extracted at a point located at a distance x of the center and so an equation $P/\text{MPa} = f(t)$ is obtained, where time $t = 0$s is defined when the polymer flow front first reaches the nanocavity. This equation and the temperature of the polymer when it reaches the nanocavity are the values used for the subsequent MD nanosimulation.

Nano-MD simulation

The model used to perform the nano-MD simulation is the one published in "Molecular dynamics simulation method applied to nanocavities replication via injection moulding"[17]. It consists in the following steps: (i) generating an initial configuration of the polymer, (ii) compressing it until the target density, (iii) minimizing and equilibrating it and, (iv) performing the production run using the pressure equation transformed into force taking into account the nanocavity entrance area. Specifically for this paper, the mould is modeled with body-centered cubic (BCC) aluminium. The polymer is enclosed with a layer of frozen BCC atoms located above it, this is an alternative to the introduction of a vacuum layer done by other authors such as Zhou[23].

The above exposed model takes into account two hypothesis:

- The replication takes place in the filling stage and the packing stage is of no influence in the degree of replication. It is stated in "3D filling simulation of micro and nanostructures in comparison to iso- and variothermal injection moulding trials"[7] that such hypothesis is acceptable as long as the mould temperature is below the No Flow Temperature of the polymer.

- Since the nanofeature is so small, the polymer initially goes through it as it was not present and, next, it gets inside the nanocavity due to the pressure profile. This was initially stated by Tofteberg[12] and experimentally proven by Pina[15].

3. RESULTS AND DISCUSSION

This section is divided into two sections corresponding to the two studied factors, the degree of polymerization and the tacticity.

3.1 Degree of polymerization effect

The degree of polymerization is the number of monomers that constitute each polymer chain. Polyethylene is used in this section, see figure 3 for an image where n refers to the degree of polymerization of polyethylene. The reason for using PE is that it is the most simple polymer and, hence, the necessary computational resources are reduced.
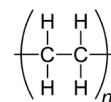
Figure 3: *The degree of polymerization is the number n of monomers constituting each PE chain.*

The degree of polymerization of PE can be controlled in the production process by adjusting the reaction conditions. D'Agnillo[24] shows a method to tune the degree of polymerization using soluble metallocene/methylalumoxane catalysts. Feucht[25] proves mathematically that the degree of polymerization decreases with increasing reaction temperature and is higher at higher residence times and smaller amounts of initiator in the feed.

Using SolidWorks Plastic an injection plastic simulation to obtain the geometry of figure 2 is performed with polyethylene (PE-MD BASELL LUPOLEN 2410 of $T_g = -125$°C and $T_m = 117$°C), where temperatures for the polymer and the mould are set to $T_{polymer} = 230$°C and $T_{mould} = 45$°C, filling time 2s and injection pressure limit of 134MPa. The pressure profile is extracted from SolidWorks simulation at x = 11.9mm and the equation $P/\text{MPa} = 1.0643t^2 + 0.1202t$ is obtained. This equation and the temperature of the polymer when it reaches the nanocavity (227°C) are the values used for the subsequent MD nanosimulations.

The MD-nanosimulations consists of a set of three simulations performed with three different degrees of polymerization (100, 500 and 800). The contour length of the polymer chain with each degree of polymerization can be calculated taking into account that the angle between the C-C bonds is 109.5° and the C-C distance equal to 0.154nm. Thus the apparent distance d (in nm) between two successive carbon atoms of the all trans chain is given by:

$$d = 0.154 \cdot \sin\frac{109.5°}{2} = 0.126\text{nm} \quad \textit{(1)}$$

The contour lengths of PE with a degree of polymerization 100, 500 and 800 are 25.2nm, 126nm and 201.6nm, respectively. The gyration radius are 0.73nm, 1.63nm and 2.06nm, also respectively. These dimensions, compared to the entrance area of $2 \cdot 2nm^2$ give an idea of how difficult it is for the polymer to get into the nanocavities.

Figure 4 shows a front image of the polymer inside the $2 \cdot 2nm^2$ cavity once it reaches the No Flow Temperature of 147ºC. It is clearly stated that longer polymer chains lead to a smaller degree of replication. In fact, the replication is reduced linearly as shown in figure 5.
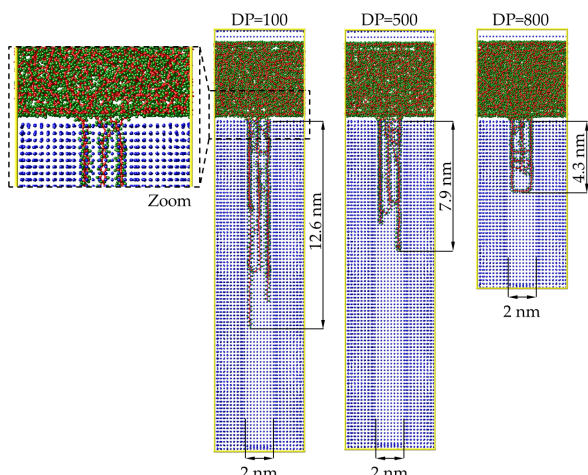

Figure 4: *Front image of the polymer once it reaches the NFT. The blue points are the aluminium atoms. A zoom is shown in order to show the atomistic detail level of the simulation.*
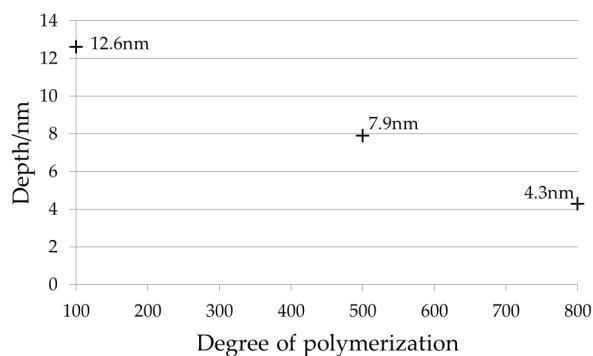

Figure 5: *Depth vs. degree of polymerization plot for the cavities with $2 \cdot 2nm^2$ sectional area. It is observed how larger degrees of polymerization hinder the polymer replication due to the entanglement of the polymer chains above the hole.*

The reason for the negative effect of the degree of polymerization in the replication is the larger entanglement that takes place with long polymer chains. Nevertheless, the replicated depth is considerable compared with the sectional area, indeed, even with the larger degree of polymerization of 800, 4.3 nm are

replicated, approximately the double of the nanocavity dimension.

The calculation time of each simulation was of approx. 75h with Intel(R) Core(TM) i5-3320M CPU @ 2.60 GHz) with 4 cores parallelization.

Tacticity effect

The purpose of this section is to study the tacticity effect on the replication. Tacticity is the relative stereochemistry of adjacent chiral centers within a macromolecule, i.e., the way the substituents are arranged along the backbone chain of the polymer.

Polystyrene is used in the simulations of this section because the phenyl substituent is voluminous and, hence, the tacticity effect can be doubtless proved. Polystyrene is manufactured by styrene polymerization. See figure 6:
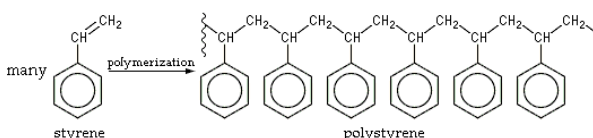
Figure 6: *Polymerization reaction of styrene.*

According to the reaction conditions, the three usual different tacticities can be obtained as shown in figure 7:

Atactic

In atactic polystyrene the phenyl groups are placed randomly along the chain. It is the commonly commercialized form of polystyrene and the polymerization is initiated with free radicals. The random positioning of the phenyl groups prevents the chains from aligning and, hence, none crystallinity is obtained, generating an irregular and amorphous polymer. Due to its amorphous characteristic, it has no T_m and T_g=100ºC.

Isotactic

In isotactic polystyrene all the phenyl groups are located on the same side of the macro-molecular backbone. It leads to a semi crystalline polymer with T_m= 240ºC and T_g=100ºC.

Syndiotactic

In syndiotactic polystyrene the phenyl groups have alternate positions along the chain. Syndiotactic polystyrene is obtained with Ziegler-Natta polymerization. This form is highly crystalline with a T_m of 270ºC and a T_g= 100ºC. It is produced under the trade name XAREC.

In this section, three simulations are performed with the submodeling approach in order to study the effect of tacticity in the replication of a $3 \cdot 3nm^2$ cavity with a single polymer chain of DP=550. The cavity length is increased in comparison with the $2 \cdot 2nm^2$ of the previous section because the voluminous phenyl

Figure 7: *Molecular structure of three different PS tacticities.*

substituent of polystyrene makes necessary a larger entrance area rather than polyethylene.

The macro simulation is performed with Solidworks Plastics with filling time=2.37s, T_{mould} = 50°C, $T_{polymer}$ = 230°C and maximum inlet pressure of 134MPa. From this simulation, the pressure in a point l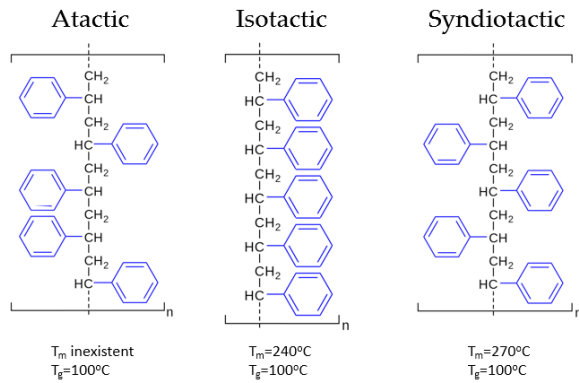ocated 12.48mm of the center is exported and the pressure profile is obtained ($P/Pa = -194991t^2 + 210580t$). The Molecular Dynamics simulation is performed and a snapshot of the polymer once it has reached the NFT is shown in figure 8.
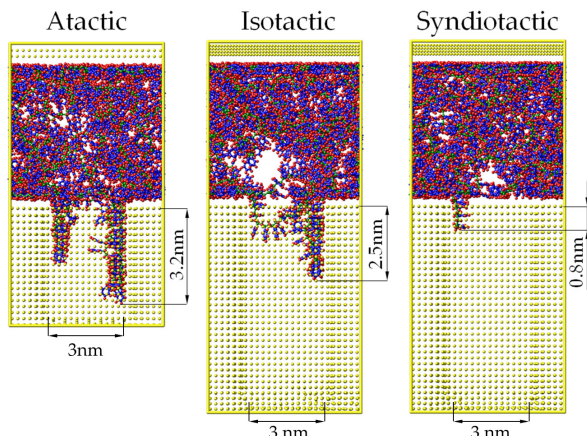

Figure 8: *Frontal image of PS once it has reached the NFT inside the nanocavity for atactic, isotactic and syndiotactic configurations. Yellow points correspond to aluminium.*

Figure 9 shows a bar chart with the replicated depth and the time elapsed until NFT for each tacticity. It is concluded that the tacticity affects the replication of the nanocavities. This is a logical result because the entanglement of the polymer chains above the nanocavity are influenced by the position of the substituent groups. Indeed, syndiotactic configuration leads to a fewer replication of the nanocavity because the alternate position of the phenyl groups eases the entanglement. Atactic PS, which is commonly commercialized, has the higher degree of replication, not far away

from the isotactic configuration. It is observed that the replication gets worse with the degree of crystallization of the polymer, indeed, the atactic configuration is amorphous, isotactic is semi-crystalline and syndiotactic is crystalline. The time until NFT shows opposite results, fewer replications lead to larger time until the NFT. This is due to the fewer contact of the polymer with the walls that takes place with smaller replications.
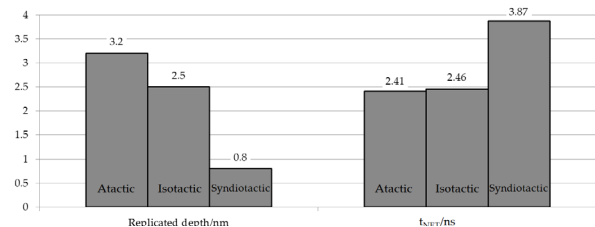
Figure 9: *Bar chart with the replicated depth and the time elapsed until the polymer reaches the NFT for atactic, isotactic and syndiotactic configurations of PS for $3 \cdot 3nm^2$ sectional area.*

The calculation time of each simulation was of approx. 100h with Intel(R) Core(TM) i5- 3320M CPU @ 2.60 GHz) with 4 cores parallelization.

CONCLUSIONS

In this paper has been proved that Molecular Dynamics simulation method enables the study of the molecular structure effect on the replication of nanostructures.

The degree of polymerization is a factor with a negative factor. Indeed, longer polymer chains lead to a smaller replication of the nanocavities due to the larger entanglement of the chains above the nanocavities. For a nanocavity with an entrance area of $2 \cdot 2nm^2$, the replication depth was of 12.6nm for DP=100, 7.9nm for DP=500 and of 4.3nm for DP=800, as shown in figure 4, 5.

Concerning the tacticity factor, it has been proved that the polymer tacticity influences the nanostructures replication. Indeed, for a $3 \cdot 3nm^2$ a syndiotactic polymer leads to a smaller replication (0.8nm) compared with an atactic (3.2nm) or isotactic (2.5nm) polymer due to the larger entanglement between adjoining chains as shown in figure 8 and plotted in the bar chart of figure 9.

REFERENCES

1. Hwajin Oh, Jaehong Park, Youngseok Song, and Jaeryoun Youn. Micro-injection Moulding of Lab-on-a- chip (LOC). 19, 2011.
2. Sohee Kim, Une Teak Jung, Soo Kyoung Kim, Joon Hee Lee, Hak Soo Choi, Chang Seok Kim, and Myung Yung Jeong. Nanostructured multifunctional surface with antireflective and anti-

microbial char- acteristics. ACS Applied Materials and Interfaces, 7(1):326–331, 2015.

3. Y. E. Yoo, T. H. Kim, D. S. Choi, S. M. Hyun, H. J. Lee, K. H. Lee, S. K. Kim, B. H. Kim, Y. H. Seo, H. G. Lee, and J. S. Lee. Injection molding of a nanostructured plate and measurement of its surface properties. Current Applied Physics, 9(2 SUPPL.):e12–e18, 2009.

4. Sunandan Baruah, Samir K Pal, and Joydeep Dutta. Nanostructured Zinc Oxide for Water Treatment. Nanoscience and Technology-Asia, 2(2):90–102, 2012.

5. Alexander B. Christiansen, Jeppe S. Clausen, N. Asger Mortensen, and Anders Kristensen. Injection moulding antireflective nanostructures. Microelectronic Engineering, 121:47–50, 2014.

6. Jae-Jun Kim, Youngseop Lee, Ha Gon Kim, Ki-Ju Choi, Hee-Seok Kweon, Seongchong Park, and Ki-Hun Jeong. Biologically inspired LED lens from cuticular nanostructures of firefly lantern. Proceedings of the National Academy of Sciences of the United States of America, 109(46):18674–8, 2012.

7. C Rytka, J Lungershausen, P M Kristiansen, and A Neyer. 3D filling simulation of micro- and nanos- tructures in comparison to iso- and variothermal injection moulding trials. Journal of Micromechanics and Microengineering, 26(6):65018, 2016.

8. Kari Monkkonen, Tuula T. Pakkanen, Joni Hietala, Esko J. Pakkonen, Pertti Pakkonen, Timo Jskelinen, and Terho Kaikuranta. Replication of sub-micron features using amorphous thermoplastics. Polymer Engineering and Science, 42(7):1600–1608, 2002.

9. Baichuan Sha, Stefan Dimov, Christian Griffiths, and Michael S. Packianather. Micro-injection mould- ing: Factors affecting the achievable aspect ratios. International Journal of Advanced Manufacturing Technology, 33(1-2):147–156, 2007.

10. Chun Sheng Chen, Shia Chung Chen, Won Hsion Liao, Rean Der Chien, and Su Hsia Lin. Micro injection molding of a micro-fluidic platform. International Communications in Heat and Mass Transfer, 37(9):1290–1294, 2010.

11. Shuntaro Hattori, Keisuke Nagato, Tetsuya Hamaguchi, and Masayuki Nakao. Rapid injection molding of high-aspect-ratio nanostructures. Microelectronic Engineering, 87(5-8):1546–1549, 2010.

12. T Tofteberg and E Andreassen. Injection moulding of microfeatured parts. Proceedings of the Polymer Processing Society 24th Annual Meeting, PPS-24, 2008.

13. Sung Joo Choi and Sun Kyoung Kim. Multiscale filling simulation of micro-injection molding process. Journal of Mechanical Science and Technology, 25(1):117–124, 2011.

14. Liyong Yu, L James Lee, and Kurt W Koelling. Flow and heat transfer simulation of injection molding with microstructures. Polymer Engineering & Science, 44(10):1866–1876, 2004.

15. Jordi Pina Estany, Carles Colominas, Jordi Fraxedas, Jordi Llobet, Francesc Perez Murano, Josep Maria Puigoriol Forcada, Dani Ruso, and Andrés Amador García Granada. A statistical analysis of nanocavities replication applied to injection moulding. International Communications in Heat and Mass Transfer, 2016.

16. Pina-Estany Jordi and García-Granada Andrés-Amador. 3D simulation of nanostructures replication via injection moulding. International Polymer Processing, 2017.

17. Jordi Pina Estany and Andrés Amador García Granada. Molecular dynamics simulation method applied to nanocavities replication via injection moulding. International Communications in Heat and Mass Transfer, 87:1–5, 2017.

18. Shigeo Maruyama. Molecular Dynamics Method for Microscale Heat Transfer. Advances in Numerical Heat Transfer, 2(Md):189–226, 2000.

19. Yuxiu Li, Jinliang Xu, and Dongqing Li. Molecular dynamics simulation of nanoscale liquid flows. Microfluidics and Nanofluidics, 9(6):1011–1031, 2010.

20. Takashi Yamamoto. Molecular dynamics modeling of polymer crystallization from the melt. Polymer, 45(4):1357–1364, 2004.

21. Chi Fu Dai and Rong Yeu Chang. Molecular dynamics simulation of thread break-up and formation of droplets in nanoejection system. Molecular Simulation, 35(4):334–341, 2009.

22. Jie Feng, Qiang Liao, Xun Zhu, Rui Wu, Hong Wang, YuDong Ding, and Kisaragi Yashiro. Molecular dynamics simulation of injection of polyethylene fluid in a variable cross-section nano-channel. Chinese Science Bulletin, 56(17):1848–1856, 2011.

23. Mingyong Zhou, Bingyan Jiang, and Can Weng. Molecular dynamics study on polymer filling into nano-cavity by injection molding. Computational Materials Science, 120:36–42, 2016.

24. Luigi D'Agnillo, João B. P. Soares, and Alexander Penlidis. A critical examination of polyethylene molecular weight distribution control through the combination of soluble metallocene/methylalumoxane catalysts. Polymer International, 47(3):351–360, 1998.

25. P Feucht and B Tilger. P. FEUCHT, B. TILGER and G. LUF"Tt. 40(6):1935–1942, 1985.

2.5 Paper V: Replication of nanoscale surface gratings via injection molding (under review)

The purpose of this work is to study the capability of injection molding to replicate nanostructured areas in regular-sized parts by means of injection molding. A chip with an array of different nanostructures is manufactured and glued into a mould. With this assembly, different sets of experiments are carried out along with a repeatability analysis in order to study the effect in the replication of process factors (maximum injection pressure, filling time, charge and polymer temperature), geometric factors (width and separation between trenches) and demolding conditions. From all the factors, the one with a larger effect is the separation between consecutive trenches, this factor is studied in detail through CFD simulation.

Atomic Force Microscope measurements of the polymer and the mould have been matched during the postprocessing and a previously not reported sinking effect of the polymer is observed and afterward analyzed through multiphysics simulations.

2.6   Paper VI: Injection moulding of plastic parts with laser textured surfaces with optical applications

The purpose of this work is to manufacture micro and nanotextured surfaces on plastic injection moulds with the aim of replicating them and obtaining plastic parts with optical applications. Different patterns are manufactured with nanosecond and femtosecond lasers in order to obtain three different optical applications: (i) homogeneous light diffusion (ii) 1D light directionality and (iii) 2D light directionality. Induction heating is used in the injections in order to improve the textures degree of replication. The steel mould and the plastic parts are analyzed with a confocal/focus variation microscope and with a surface roughness tester. A mock-up and a luminance camera are used to evaluate the homogeneity and luminance of the homogeneous light diffusion application in comparison with the current industrial solutions.

https://doi.org/10.1016/j.optmat.2018.03.049

Chapter 3

Results and discussion

In this section an overview of the different results obtained during the development of this thesis and in-depth exposed in the six publications are presented along with its discussion.

From the simulation point of view, the submodeling approach was used to quantify the effect of the mould and melt temperature, nanocavity geometry and filling time. A Design of Experiments 2^4 was pursued and the results of table 3.1 were obtained, where L and H dimensions are the length and the replicated depth of the nanocavity as shown in figure 3.1. The results are depicted in a form of a Pareto analysis in figure 3.2.
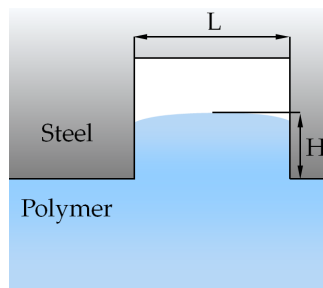

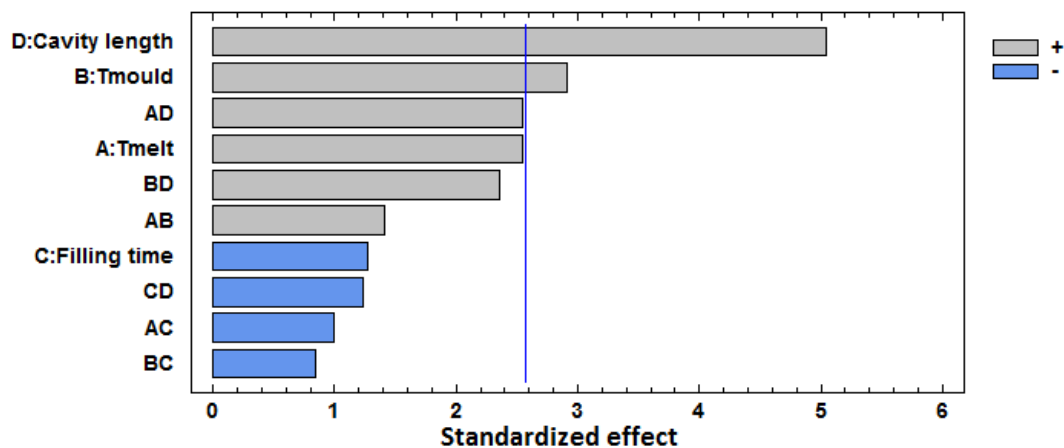FIGURE 3.1: Length (L) and height (H) dimensions of the DOE.

FIGURE 3.2: Pareto results of the DOE. Image from paper I (Pina [5]).

It is observed that the cavity length, the mould temperature and the polymer temperature have standardized effects of 5, 3 and 2.6, respectively. Filling time has a negative 1.3 standardized effect.

TABLE 3.1: Series of simulations. Table from paper I (Pina [5]).

	T_{melt}/ºC	T_{mould}/ºC	t/s	L/nm	H/nm
1	250	70	1	1000	5.0
2	310	70	1	1000	5.0
3	250	100	1	1000	55.0
4	310	100	1	1000	55.0
5	250	70	3	1000	0.0
6	310	70	3	1000	0.0
7	250	100	3	1000	55.0
8	310	100	3	1000	55.0
9	250	70	1	2000	170.0
10	310	70	1	2000	420.0
11	250	100	1	2000	412.3
12	310	100	1	2000	1500.0
13	250	70	3	2000	131.5
14	310	70	3	2000	308.3
15	250	100	3	2000	350.7
16	310	100	3	2000	762.5

The factor with the biggest effect is the geometry of the mark. It is broadly shown in the literature that cavities with small aspect ratio are more difficult to fill, reason is the surface-to-volume ratio leads to an increase of the heat transfer and, hence, to a faster solidification of the polymer (Piotter [16], Chen [17]). We see that both temperature of the mould and temperature of the melt are factors that help similarly the replication of the marks. This is a logic result since the marks are copied until the polymer reaches the glass transition temperature, hence, the bigger the mould and melt temperatures, the bigger the time the polymer has to go into the mark before reaching its glass transition temperature. Besides, the bigger the temperature, the less viscous the polymer is and the easier it goes into the marks. Related to the filling time, it is seen that the increase of the filling time leads to a fewer replication of the mark, the reason is that shorter filling times lead to larger pressures in the nanocavity macro-CFD simulation.

Experimentally, the patterns G and P are engraved (see figure 3.3) and once the obtained plastic part is evaluated with the AFM, three important results are obtained (see figure 3.4). First, the polymer replicates more when the marks are bigger (G2 compared to P2), this is in agreement with the simulation results, where it was stated that the cavity length is a factor with a positive effect. And, second, the shape and the depth reached by the polymer in the cross shaped cavities is the same for both directions: parallel and perpendicular to the polymer flow. This experimental observation reinforces the two stages hypothesis in which the simulations are based.

The CFD-based submodeling approach is expounded to the 3D and it is seen that 2D simulations are not accurate when applied to a nanocavities with a length/width<4 (see figure 3.5). In such geometries, the heat transfer is relevant in the four walls that surround the nanocavity.

Apart from this casuistic, the 3D model is necessary when the final shape of the polymer in the two directions is of interest. However, as statted in figure 3.6
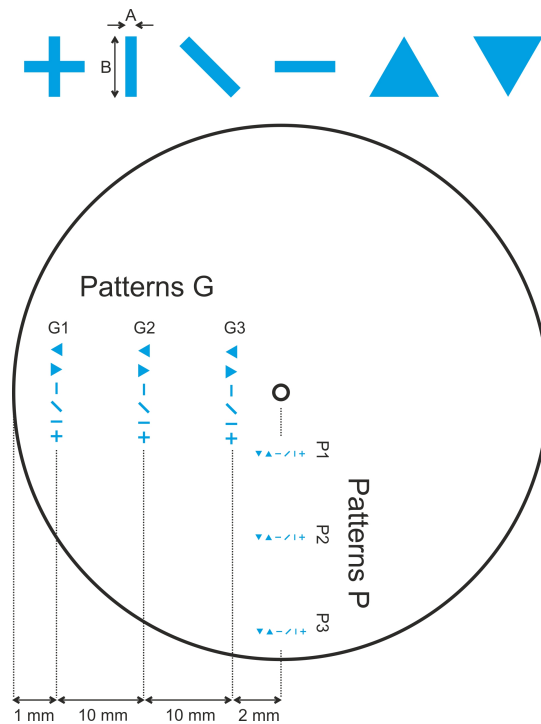
FIGURE 3.3: Designed FIB marks and their position for mould (not to scale). The diameter of the piece is 50 mm and the dimensions of patterns G and P are: $A = 4\mu$m, $B = 20\mu$m and $A = 2\mu$m and $B = 10\mu$m, respectively. Figure from paper I (Pina [5]).
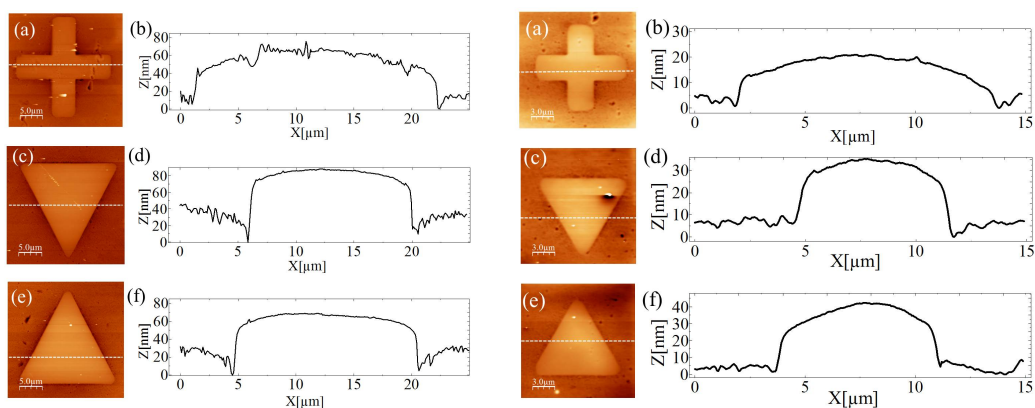
(A) Transferred G2 patters at the centre of the mould and corresponding cross sections

(B) Transferred P2 patterns at the centre of the mould and corresponding cross sections.

FIGURE 3.4: AFM measurements of G2 and P2 patterns transferred in the plastic parts. Figure from paper I (Pina [5]).

FIGURE 3.5: Convergence of 2D results to 3D results for $L/W > 4$.
Figure from paper II (Pina [7]).

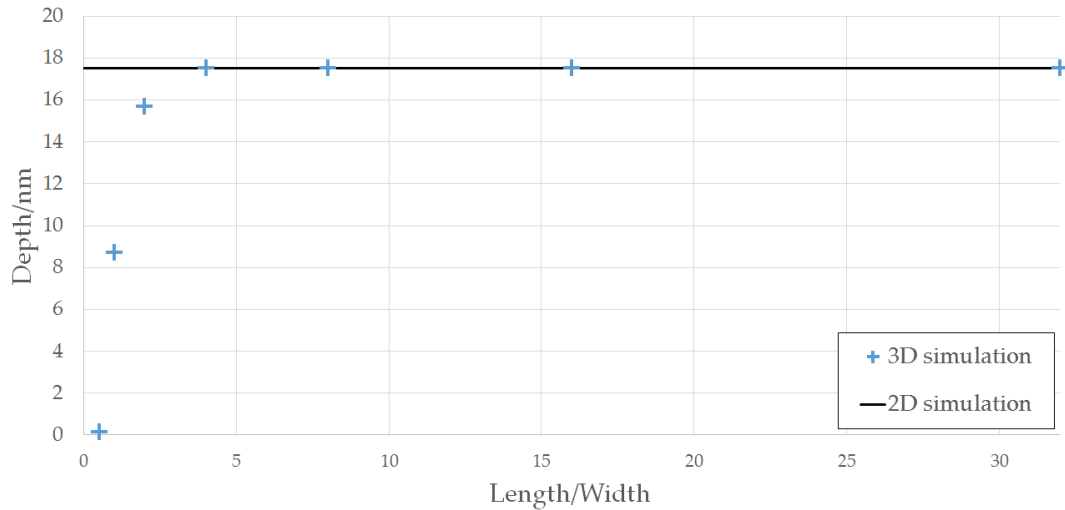it has been found that the simulation factor with a larger effect in the polymer final shape is the Mushy constant. The A_{mush} parameter defines how fast the polymer stops moving when it reaches the solidification temperature and is is not possible to know what A_{mush} parameter should be used without having previous experimental results.
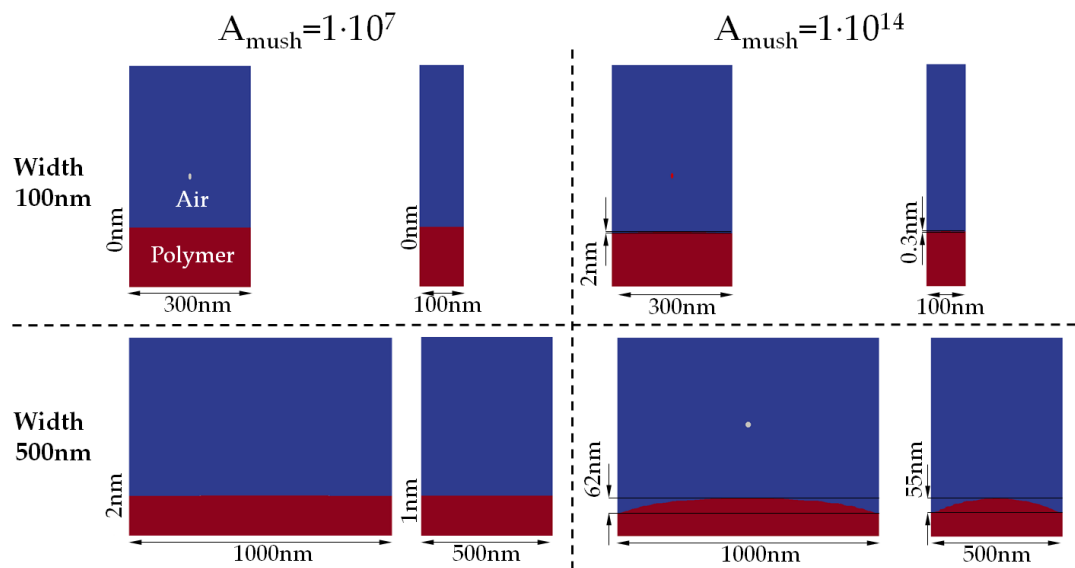
FIGURE 3.6: Dependence of the final shape with the Mushy number and the cavity geometry. Figure not to scale. Figure from paper II (Pina [7]).

When Molecular Dynamics simulation method is used to overcome the continuum limitation of the CFD, several results are obtained. When analyzing the effect of the entrance area, it is proven from the molecular point of view that smaller entrance areas lead to larger heat transfer coefficients and to less atoms inside the cavity when the polymer temperature reaches the NFT. See table 3.2. In fact, it is found out that there is a threshold entrance area from which the replication is completely unsuccessful.

TABLE 3.2: Results of the four simulations carried out with different nanocavities entrance area. Table from paper III (Pina [6]).

Nanocavity area/nm^2	Atoms at t_{NFT}	$t_{replication}$/ns	t_{NFT}/ns	HTC/$Wm^{-2}K^{-1}$
$0.62 \cdot 0.62$	4l | No replication			
$1.6 \cdot 1.6$	372	0.065	0.62	$3.27 \cdot 10^5$
$2.3 \cdot 2.3$	730	0.025	0.68	$2.95 \cdot 10^5$
$3 \cdot 3$	1766	0.015	1.4	$2.37 \cdot 10^5$

Related to the replication, it is also observed in figure 3.7 that the replication of the cavity stops far before the polymer reaches the NFT. Indeed, it is seen that the entanglement of the polymer chains above the nanocavity hinders the replication before it completely solidifies.
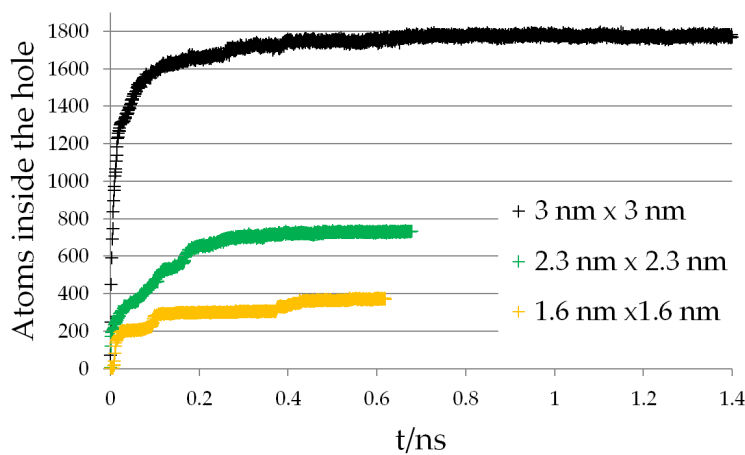

FIGURE 3.7: Evolution of the number of atoms inside the cavity. The number of atoms stabilizes far before the polymer reaches the NFT. Figure from paper III (Pina [6]).

The polymer molecular structure effect is studied and it is observed that the tacticity of PS effects its replication (see figure 3.8). This is a logical result because the entanglement of the polymer chains above the nanocavity are influenced by the position of the substituent groups. Indeed, syndiotactic configuration leads to a fewer replication of the nanocavity because the alternate position of the phenyl groups eases the entanglement. Atactic PS, which is commonly commercialized, has a higher degree of replication, not far away from the isotactic configuration. It is observed that the replication gets worse with the degree of crystallization of the polymer, indeed, the atactic configuration is amorphous, isotactic is semi-crystalline and syndiotactic is crystalline. The time until NFT shows opposite results (see figure 3.9), fewer replications lead to larger time until the NFT. This is due to fewer contact of the polymer with the walls that take place with smaller replications.

The degree of polymerization is also studied with PE of three different DP: 100, 500 and 800. Figure 3.10 shows a front image of the polymer inside the $2 \cdot 2nm^2$ cavity once it reaches the No Flow Temperature of $147\,^{\circ}$C. It is clearly stated that longer polymer chains lead to a smaller degree of replication. This is due to larger entanglement of longer polymer chains.

Experimentally, photolitography and RIE was used to manufacture a chip with the several geometries depicted in figure 3.11.
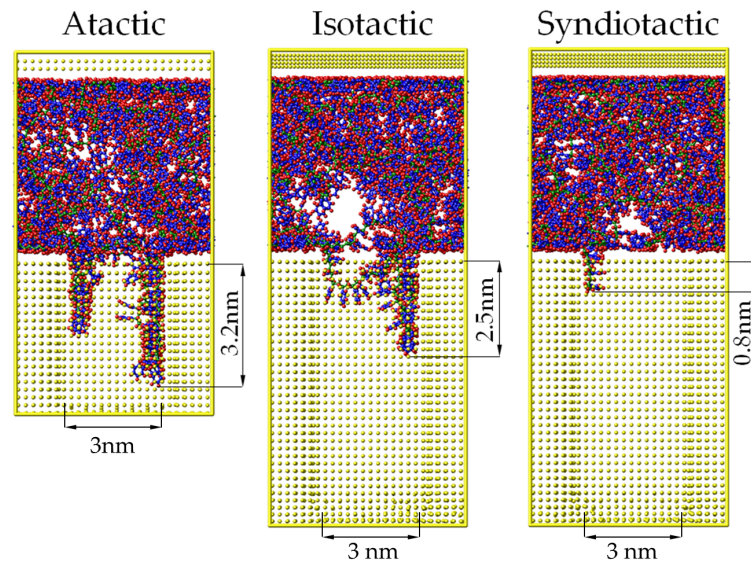
FIGURE 3.8: Frontal image of PS once it has reached the NFT inside the nanocavity for atactic, isotactic and syndiotactic configurations. Yellow points correspond to aluminium. Figure from paper IV (Pina [8])
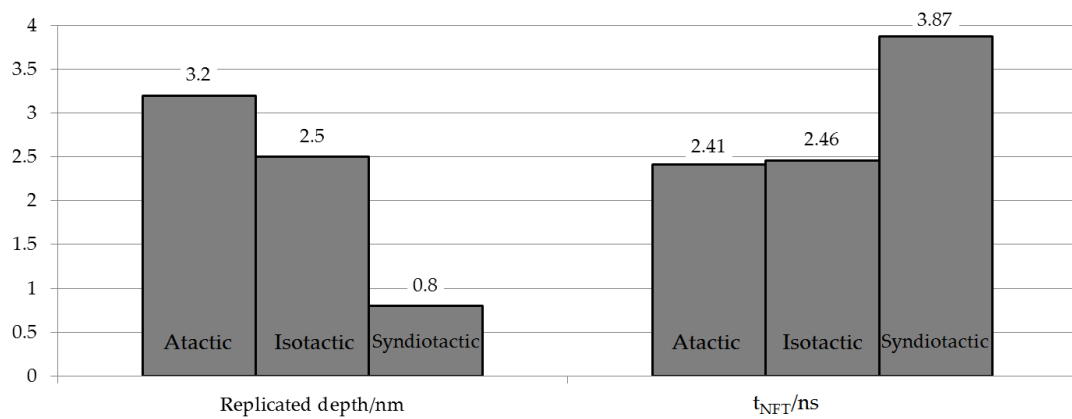
FIGURE 3.9: Bar chart with the replicated depth and the time elapsed until the polymer reaches the NFT for atactic, isotactic and syndiotactic configurations of PS for $3 \cdot 3\,\text{nm}^2$ sectional area. Figure from paper IV (Pina [8]).
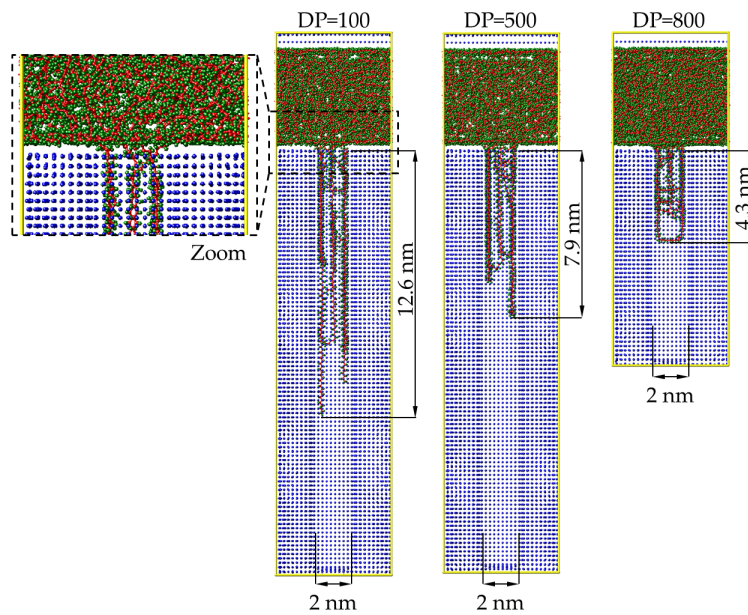
FIGURE 3.10: Front image of the polymer once it reaches the NFT. The blue points are the aluminium atoms. The zoom shows the atomistic detail level of the simulation. Figure from paper IV (Pina [8])
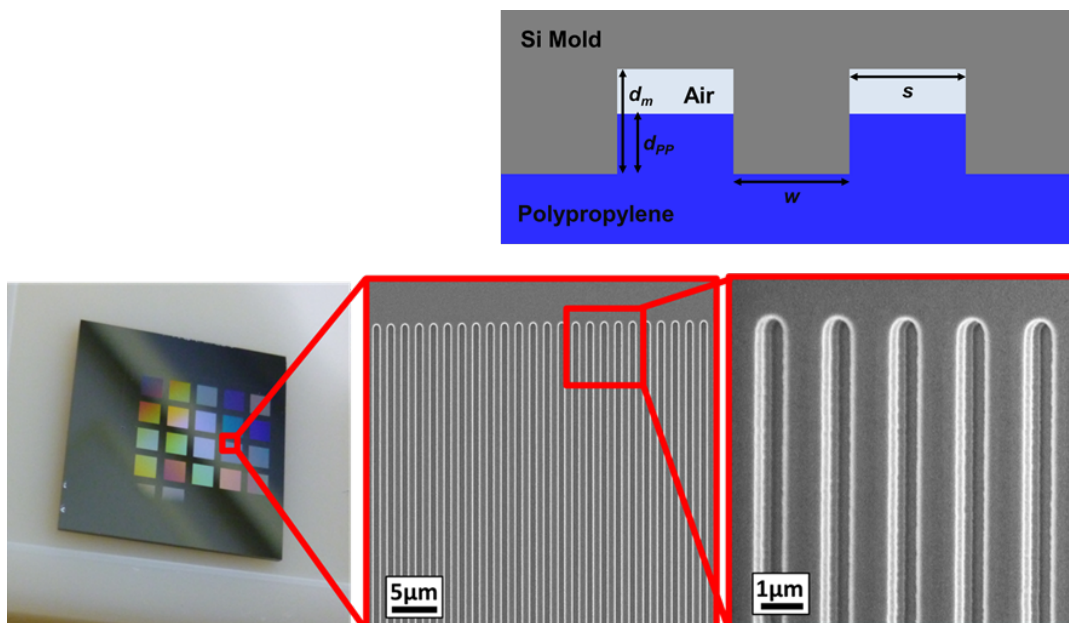
FIGURE 3.11: Upper right: Schematic of micro/nanostructures on the mold and polypropylene part during the injection process. w and s refer both to the plastic and mold dimensions while d_m is the depth of the mold and d_{PP} is the maximum depth reached by the polypropylene. Bottom: Photograph and SEM images of the silicon chip used for the injections. Figure from paper V ([2]).

A set of experiments was designed to investigate the following parameters: maximum inlet pressure (P), filling time (t), charge (material intake, measured as a stroke of the pushing cylinder), polymer temperature (T), width of the trenches (w) and separation between them (s). Polymer parts were manufactured with five different process conditions (A to E) as described in figure 3.12. The replication depth of the trenches is measured for four combinations of w and s by AFM.
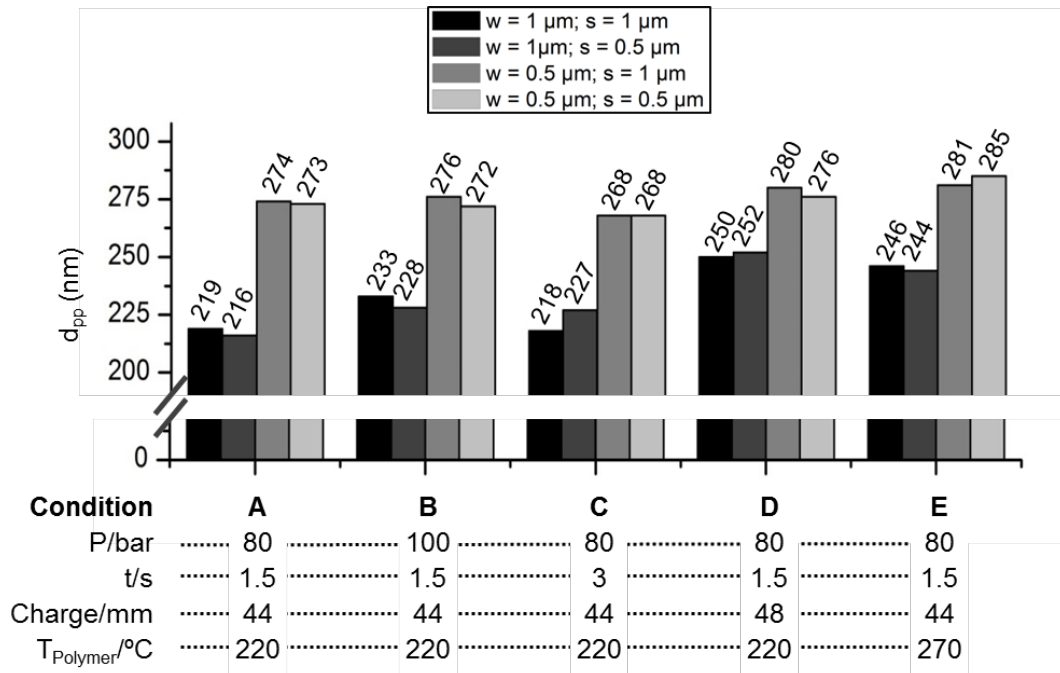

FIGURE 3.12: Set of experiments to quantify the effect of four factors in the nanocavities replication (maximum inlet pressure, filling time, charge and polymer melt temperature). Figure from paper V ([2]).

It is clearly observed in figure 3.13 that the geometrical factor with a major effect on the height of the replicated plastic nanostructures is the distance between consecutive trenches (w): the smaller it is, the deeper the polymer gets into the cavities. This was studied by means of CFD submodeling algorithm and it was found out that smaller w leads to a warming of the mould steel between trenches. Thus, it is like injecting the polymer at a larger mould temperature, what was already proven to be a factor that effects the replication positively (see figure 3.13).

When the polymer and the mould AFM lectures were superposed, a sinking effect and a shrinking of the pattern period were found out at the light of figure 3.14.

The reason for the mentioned sinking is that air is trapped in the cavities of the mold once the polymer has completely covered the cavity entrance. The advance of the melted polymer in the cavities compresses the trapped air, thus increasing its pressure following the Boyle's law [12] and, therefore, hindering the polymer progress. This effect is experimentally studied for the different geometries and process conditions (3.15) and it is proved to be more pronounced in patterns with smaller trench separation (w) where the polymer is at higher temperature; first because the polymer fills more fraction of the cavity than for larger w and, therefore the pressure increases more and, second, because
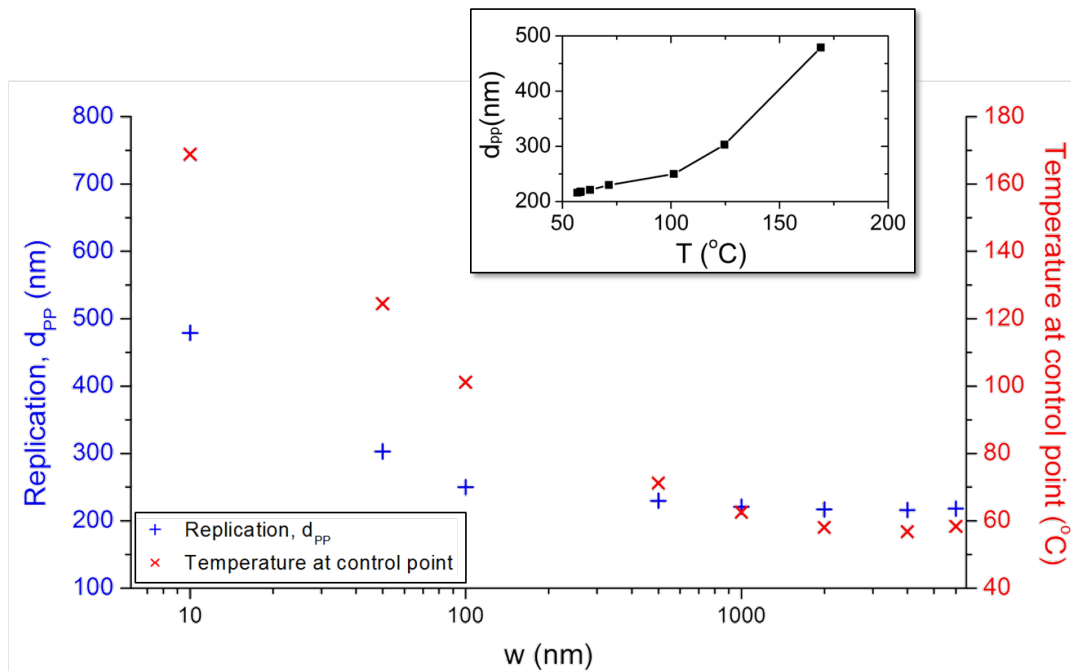
FIGURE 3.13: Simulated results of the impact of w in the replication of nanocavities. For $w < 1$ μm a clear tendency can be observed: smaller w leads to higher temperatures at the control point (red) and higher replications (blue). On the other hand, this tendency was not observed for $w > 1$ μm. Inset: Simulation of the depth reached by the polymer depending on the temperature. Figure from paper V ([2]).

FIGURE 3.14: Superposed AFM cross sections of the polymer (red) and mold (black) at the flow entry (left) and exit (right) of the pattern. Nominal structural parameters: $w = 0.5$ μm and $s = 1$μm. Conditions: Polymer charge = 48 mm; Pressure = 80 bar; Injection time = 1.5 s; Temperature = 200 °C. Figure from paper V ([2]).

at higher temperatures the Young's modulus is lower and thus the polymer is more easily deformed.
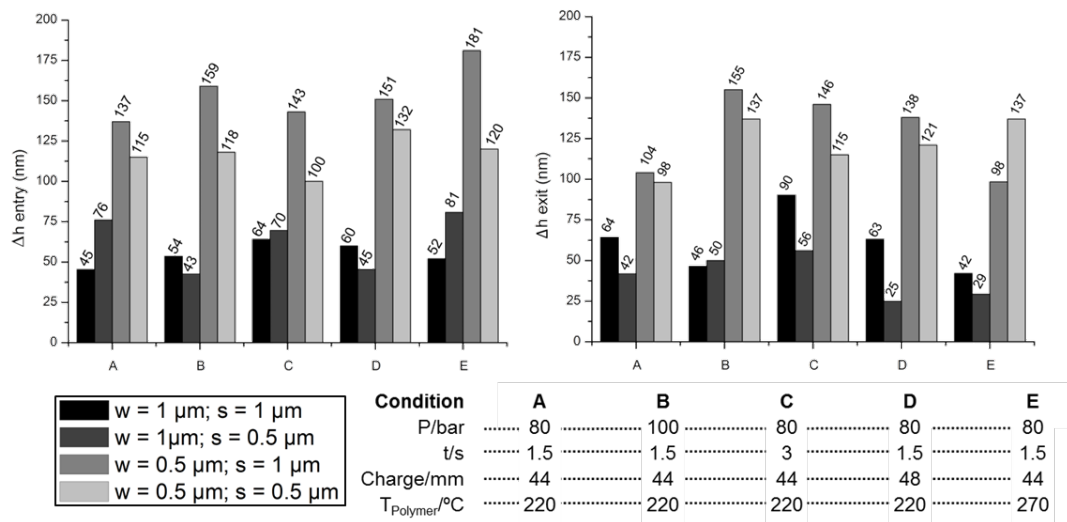
FIGURE 3.15: Study of the sinking effect at the entry and at the output of the chip for different process conditions. Figure from paper V ([2]).

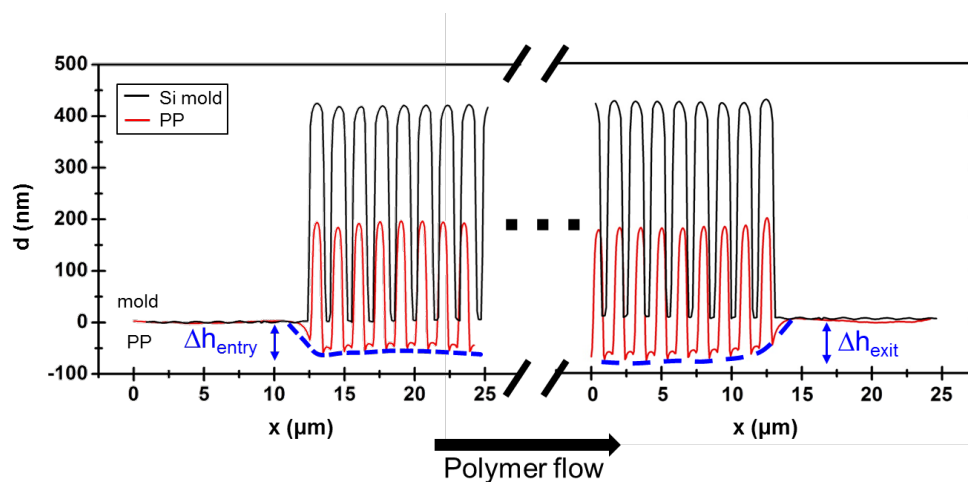Concerning to the shrinking of the pattern, the period of the mold trenches exceeds the period of the plastic trenches due to differential thermal contraction of the plastic part once it is taken out of the mold. Thermal expansion coefficient for polypropylene was set to $1.6 \cdot 10^{-4} \mathrm{K}^{-1}$ and to $1.6 \cdot 10^{-5} \mathrm{K}^{-1}$ for the silicon chip, which is 10 times smaller (Thermal expansion of steel is similar to silicon, $2 \cdot 10^{-5} \mathrm{K}^{-1}$).
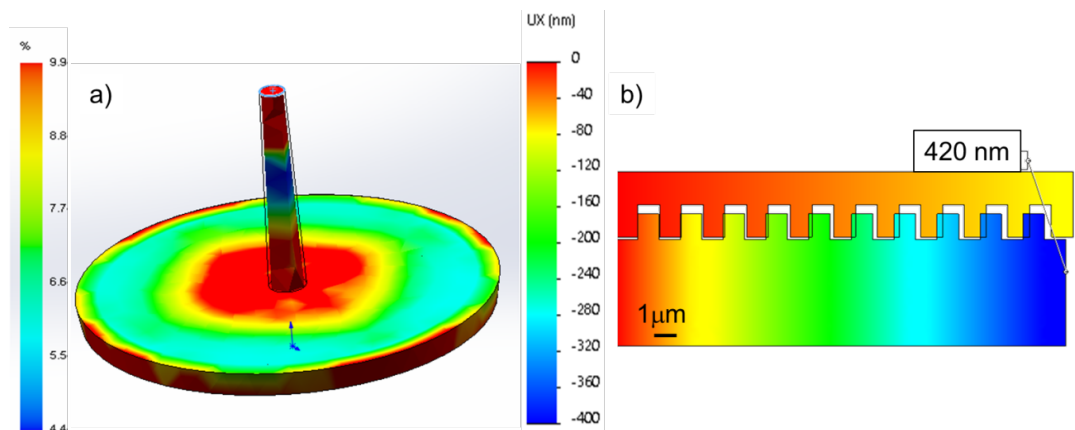
FIGURE 3.16: (a) Volume shrinking simulation with conventional plastic injection simulation and (b) thermal contraction of steel mold with silicon chip top compared to plastic part bottom to justify different period in trenches. Figure from paper V ([2]).

Experiments were carried out to study if the demolding conditions affect the replication of the cavities. In the first one, (A), the piece is extracted without waiting; in the second one, (B), the piece is extracted after one minute with the mold separated; in the third one, (C), the piece is extracted after one minute with the mold in contact.
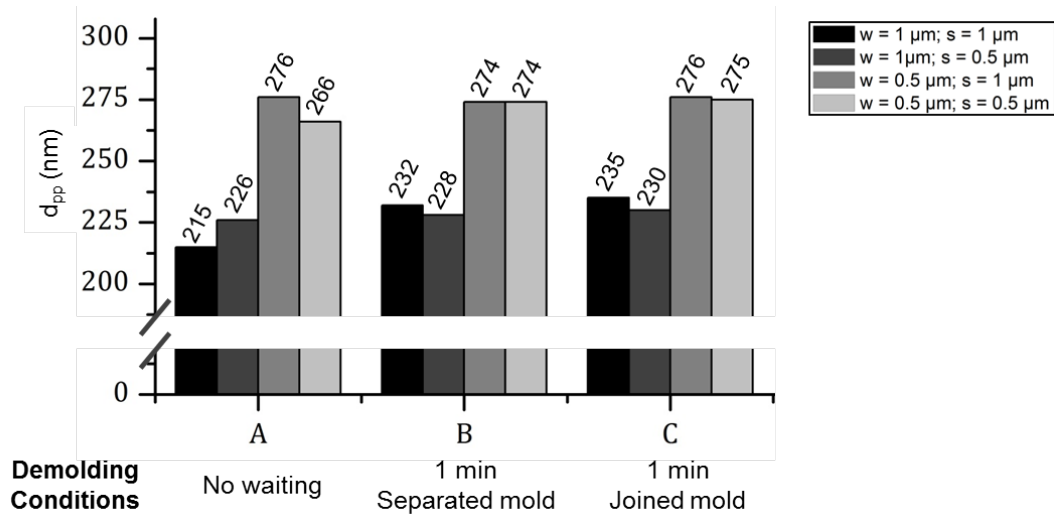
FIGURE 3.17: Study of demolding conditions in the replication of nanocavities. Figure from paper V ([2]).

Results shown in 3.17 state that the demolding conditions do not affect the value of the height in the replication. This is a relevant result from the industrial point of view because it shows that the molding cycle time can be kept at its minimum without deterioration of the nanocavities replication.

In order to investigate the precision of the tests, a repeatability analysis was performed. A total of 12 parts, 6 at 220 °C (A) and 6 more at 270 °C (B) were injected for the equivalent four combinations of w and s. The average standard deviation (1) of the height measurements was of 4.4 nm, that confirms that the replication process is repeatable and that the observed behavior is significant. See figure 3.18.
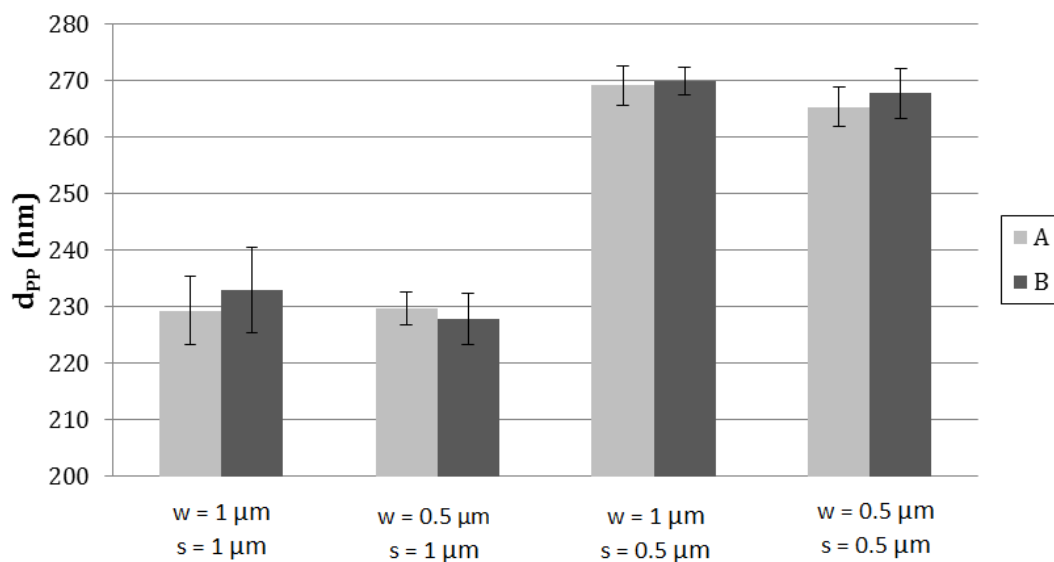
FIGURE 3.18: Results of the repeatability analysis. Figure from paper V ([2]).

Finally, from the point of view of the final application of this thesis, a common work between IQS and SEAT led to several industrial applications. First

of all, it was found out that it is possible to achieve light homogeneity when a random nanotexture is engraved in a mould with a nanosecond laser with wavelength 1064 nm, pulse duration 200 ns, repetition rate 80 kHz, optical diameter 0.07 mm, points density 300 $\mathrm{points/mm^2}$ and injected with induction heating warming method. Indeed, when Power TOP LEDs are located at 12.7 mm between them and its luminance evaluated at a distance between the LED and the light surface of 40, 35, 30 and 25 mm, the luminance plot of figure 3.19 is obtained when neither a nanotexture nor a conventional diffuser is placed.
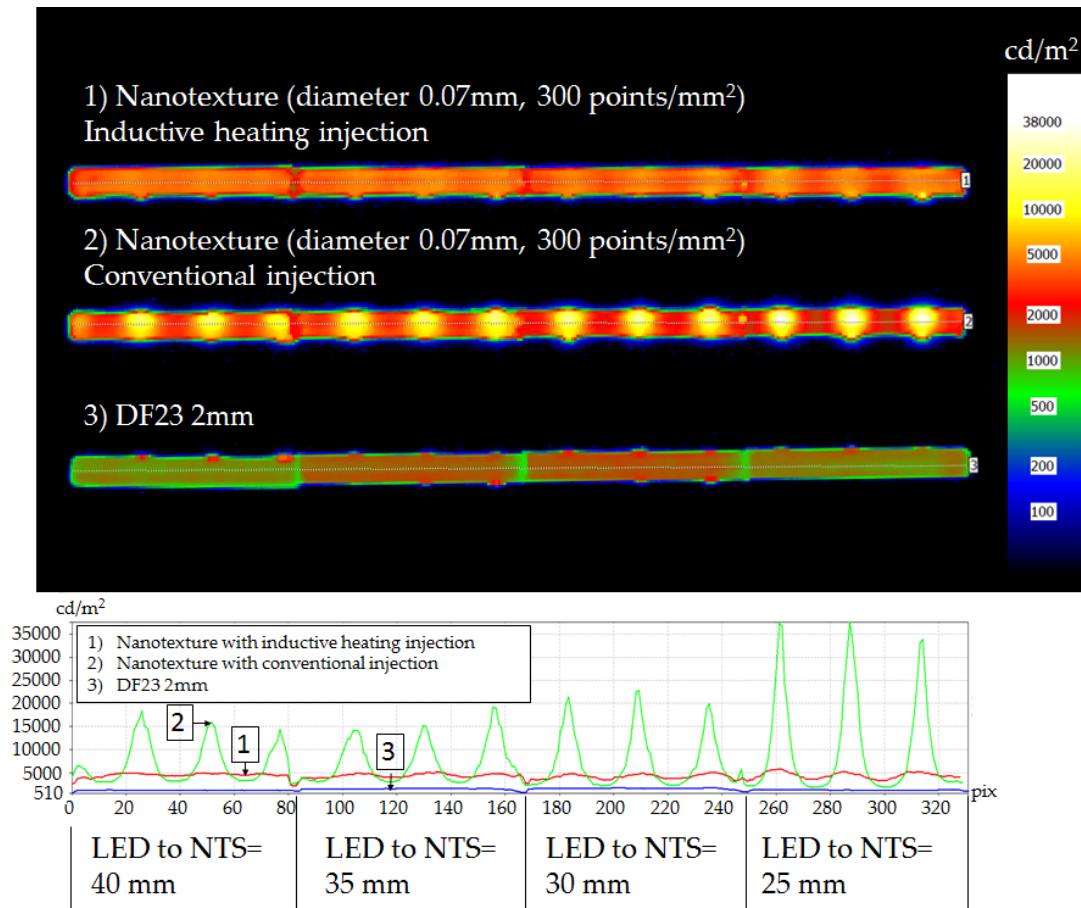
FIGURE 3.19: : Luminance images and luminance plots of nanotexture with optical diameter 0.07 mm and 300 $\mathrm{points/mm^2}$ and connected at 8 V. The four areas match with the four distances between LED and NTS or DF23 defined in the mockup, from left to right: 40 mm, 35 mm, 30 mm and 25 mm. Figure from paper VI (Pina [4]).

In table 3.3 the results of mean luminance and homogeneity are shown for the several experiments. First, it is observed how, without a NTS or a diffuse material (result 0) the mean luminance is very large (14460 $\mathrm{cd/m^2}$) in exchange of a very poor homogeneity of only 0.3%. When comparing the nanotextures results (results 1 and 2), it is observed that induction heating leads to a large improvement of the homogeneity (37.2% compared to 4.7%) at the expense of a mean luminance reduction (4292 $\mathrm{cd/m^2}$ compared to 7694 $\mathrm{cd/m^2}$). Finally, when the industrially used DF23 (result 4) is compared to the nanotexture with induction heating (result 3), it is observed how the NTS leads not only to a larger homogeneity (37.2% in comparison to 30.2%) but also to a larger mean luminance (7694 $\mathrm{cd/m^2}$ compared to 1288 $\mathrm{cd/m^2}$). The larger efficiency

TABLE 3.3: Mean luminance and homogeneity results for the different experiments. Table from paper VI (Pina [4]).

	Mean luminance/(cd/m^2)	Homogeneity
0) Only PMMA (no NTS, no DF23)	14460	0.3%
1) Nanotexture, conventional injection	7694	4.7%
2) Nanotexture, inductive heating injection	4292	37.2%
3) DF23 2 mm	1288	30.2%

of the NTS injected with induction heating leads to a possible cost-reduction of the applications aiming to obtain light homogeneity since less LEDs would be necessary to achieve a given luminance.

With the use of Refractive Optical Elements, 1D light directionality and 2D light directionality are achieved (see figure 3.20). 1D light directionality makes possible a reduction of LEDs necessary to enlighten a given area. The 2D light directionality makes possible several design applications, since given figures like logos can be projected.
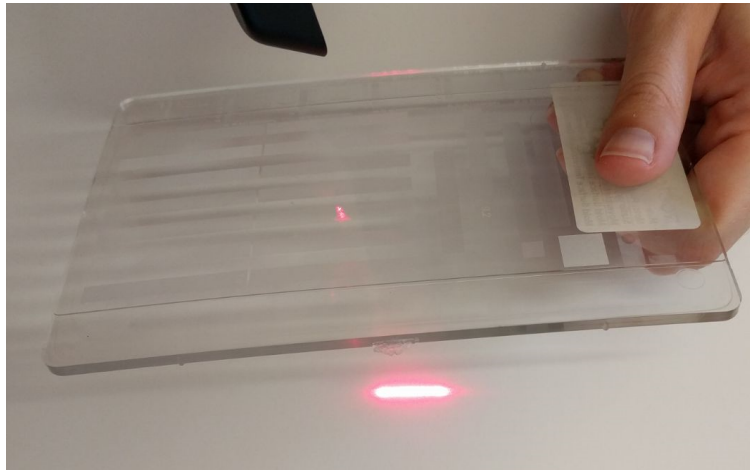
(A) 1D light directionality. The laser point is transformed into a line as it goes through the nanotexture.
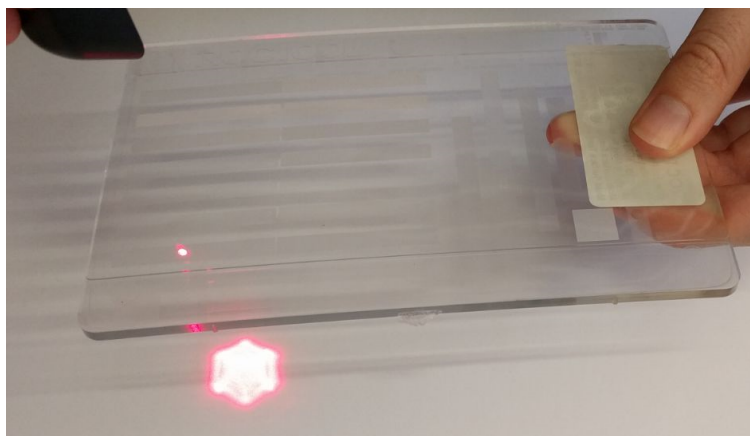
(B) 2D light directionality. The laser point is transformed into an hexagon as it goes through the nanotexture.

FIGURE 3.20: Light directionality via femtosecond manufactured NTS examples. Figures from paper VI (Pina [4]).

Chapter 4

Conclusions

The main purpose of this thesis has been accomplished, that is, injection moulding has been proved to be a cost-efficient suitable method to manufacture plastic parts with micro and nanostructured areas. During the years that lasted the research, a large amount of knowledge regarding how to improve the replication of nanocavities has been developed both experimentally and also via simulation. Such knowledge is gathered in the six publications that constitute the core of this thesis, five of them published in peer-reviewed journals and the number V currently under review. Thanks to the previously generated knowledge and to the IQS and SEAT lighting department common effort, an industrial application based on the obtaining of light homogeneity in a less expensive and more efficient way than the current methods has been developed. Next, the specific conclusions are enumerated:

– It is concluded that the CFD-based submodeling approach is a valid approach to simulate how nanocavities are filled in the injection moulding manufacturing process. Its funding hypothesis, i.e., that the the polymer goes through the nanocavity without even noticing its presence during the filling of the macro part is proved to be correct since cross shaped cavities are filled equally in the perpendicular and the parallel directions to the flow.

– Using the CFD-base submodeling approach and a Design of Experiments, the standardized effects values of the cavity length, the mould temperature and the polymer temperature were quantified to 5, 3 and 2.6 respectively. The filling time is a factor with a negative standardized effect of -1.3.

– It is concluded, thanks to the expansion of the CFD-based submodeling approach, that simulations carried out in cavities with a length/width smaller than 4, need to take into account the heat transfer in the four directions and, hence, a 3D approach must be taken into account in order to avoid a polymer replication overestimation. The 3D simulations prove to be capable to simulate the final shape of the polymer once solidified, however, these results are dependent on the A_{mush} constant, which is a value not available in the literature and should be estimated using experimental data. It is also observed that when the width dimension is increased, the polymer paraboloid shape increases.

– Molecular Dynamics simulation method has been proved capable to overcome the continuum hypothesis limitation, even at a larger computational cost. The self developed MD-based submodeling approach is proved to

be capable to quantify process parameters (injection pressure limit, filling time, polymer material, mould material, polymer temperature and mould temperature) and geometric parameters (location of the cavities in the mould and cavities geometry).

– It is proved by means of Molecular Dynamics simulations that the entrance area of cavities affects its replication, even hindering it completely below a given threshold entrance area. It is observed that the number of atoms inside the cavities reaches a constant value far before the polymer cools down to the NFT due to the entanglement of the polymer chains above the nanocavities. Smaller cavities lead to larger HTC values due to the larger surface to volume relation. Cavities with smaller entrance areas have large pressure loss and need more time to achieve a complete replication, even though the NFT is reached faster after it due to the larger surface to volume ratio.

– It is proved that the degree of polymerization is a factor with a negative effect. Indeed, longer polymer chains lead to a smaller replication of the nanocavities due to the larger entanglement of the chains above the nanocavities. For a nanocavity with an entrance area of $2 \cdot 2 \, \mathrm{nm}^2$, the replication depth was of 12.6 nm for DP=100, 7.9 nm for DP=500 and of 4.3 nm for DP=800.

– It is proved that the tacticity factor effects the nanostructures replication, indeed, for a $3 \cdot 3 \, \mathrm{nm}^2$ a syndiotactic polymer leads to a smaller replication (0.8 nm) compared to an atactic (3.2 nm) or isotactic (2.5 nm) polymer due to the larger entanglement between adjoining chains.

– When injection moulding is pursued in nanocavities of different geometries, it is concluded that the width of the trenches in the mold is a factor with no significance in the investigated dimensions range (between 0.5 and 1 μm) However, the trench separation plays a key role in the dimensions of the features in the plastic part: closer trenches lead to major heat transfer and thus to a more accurate polymer replication. The trench separation effect was found to be significant for w below 1 μm, as corroborated by Computational Fluid Dynamics simulations.

– When the plastic parts and the moulds AFM measurements were overlapped, it was found a sinking in the nanostructured area of the polymer part ranging from 25 to 180 nm depending on the injection molding conditions. This sinking effect is concluded to be a combined effect of the pressure effectuated by the trapped air in the pattern area and the local lowering of polymer Young's modulus in this region.

– It was observed a mismatch between the plastic part and the mould steel when both parts were analyzed in the AFM. This was proved by CFD simulation to be caused by the larger thermal expansion coefficient of polypropylene ($1.6 \cdot 10^{-4} \, \mathrm{K}^{-1}$) than silicon ($1.6 \cdot 10^{-5} \, \mathrm{K}^{-1}$).

– Concerning the demolding conditions, no difference in the replication accuracy was found between extracting the part from the mold without waiting, after one minute with the mold opened or after one minute with the mold closed.

– It is concluded that mass production of plastic parts with MTS and NTS for optical applications is feasible when laser ablation and induction heating injection system technologies are combined. Indeed, three different

optical applications have been manufactured: (i) homogeneous light diffusion (ii) 1D light directionality and (iii) 2D light directionality. Homogeneous light diffusion is successfully achieved when a random nanotexture is engraved with the nanosecond laser with wavelength 1064 nm, pulse duration 200 ns, repetition rate 80 kHz, optical diameter 0.07 mm, points density 300 $\mathrm{points/mm^2}$ (average distance between points of 58 µm). Without either DF23 nor nanotexture, 70000 cd are obtained in front of each LED, with an homogeneity of 0.3%. The NTS injected with induction heating leads to a better homogeneity than the NTS injected with conventional warming (37.2% compared to 4.7%). Moreover, the NTS injected with induction heating is more homogeneous than the mainly used 2 mm of DF23 (37.2% in comparison to 30.2%) and also more efficient (mean luminance of 4292 $\mathrm{cd/m^2}$ in comparison to 1288 $\mathrm{cd/m^2}$).

– In order to obtain 1D light directionality, refractive optical elements consisting in an array of trenches of 8.3 µm depth and 55 µm period are manufactured in the mould with the femtosecond laser (wavelength 1030 nm, pulse duration below 400 fs, repetition rate 500 kHz, optical diameter 0.05 mm) and successfully replicated in the plastic part. A successful light directionality effect is observed transforming light into lines of light.

– In order to obtain 2D light directionality, refractive optical elements consisting in hexagons of period 108 µm and 10 µm are manufactured with a femtosecond laser (wavelength 1030 nm, pulse duration below 400 fs, repetition rate 500 kHz, optical diameter 0.03 mm). A successful light directionality effect is observed, transforming light into hexagons.

Chapter 5

Bibliography

This bibliography includes the citation of the thesis specific chapters (Introduction, Results and discussion and Conclusions). The 126 citations contained in the six papers of the "Publications derived from this thesis" section can be found in each publication.

[1] Nonjabulo P. Gule, Nusrat M. Begum, and Bert Klumperman. Advances in biofouling mitigation: A review. *Critical Reviews in Environmental Science and Technology*, 46(6):535–555, 2016.

[2] Olga Muntada-Lopez, Pina-Estany Jordi, Carles Colominas, Jordi Fraxedas, Francesc Perez-Murano, and Andrés García-Granada. Replication by injection moulding of nanoscale surface gratings. *Microelectronic Engineering*, 2018.

[3] Lonnie Lucas and Jim Zhang. Femtosecond laser micromachining: a back-to-basics primer. *Industrial-lasers. com*, 2012.

[4] J Pina-estany, A A García-granada, and E Corull-massana. Injection moulding of plastic parts with laser textured surfaces with optical applications. 79(March):372–380, 2018.

[5] Jordi Pina Estany, Carles Colominas, Jordi Fraxedas, Jordi Llobet, Francesc Perez Murano, Josep Maria Puigoriol Forcada, Dani Ruso, and Andrés Amador García Granada. A statistical analysis of nanocavities replication applied to injection moulding. *International Communications in Heat and Mass Transfer*, 2016.

[6] Jordi Pina Estany and Andrés Amador García Granada. Molecular dynamics simulation method applied to nanocavities replication via injection moulding. *International Communications in Heat and Mass Transfer*, 87:1–5, 2017.

[7] Jordi Pina-Estany and Andrés-Amador Garc\'\ia-Granada. 3D Simulation of Nanostructures Replication via Injection Molding. *International Polymer Processing*, 32(4):483–488, 2017.

[8] Dr. García-Granada Andrés-Amador Pina-Estany Jordi. Computational analysis of polymer molecular structure effect on nanocavities replication via injection moulding. *Afinidad*, 2018.

[9] PlasticPortal. No Title.

[10] Plastics – the Facts 2014/2015.

[11] Global Plastic Production Rises, Recycling Lags.

[12] Thermoforming Wikipedia.

[13] Blow molding Wikipedia.

[14] The Plastic Professionals Website.

[15] Injection Molding.

[16] Yasitha L Hewakuruppu, Leonid A Dombrovsky, Chuyang Chen, Victoria Timchenko, Xuchuan Jiang, Sung Baek, and Robert A Taylor. Plasmonic pump–probe method to study semi-transparent nanofluids. *Applied optics*, 52(24):6041–6050, 2013.

[17] Ph Buffat and Jean Pierre Borel. Size effect on the melting temperature of gold particles. *Physical review A*, 13(6):2287, 1976.

[18] Jiang Wu, Peng Yu, Andrei S Susha, Kimberly A Sablon, Haiyuan Chen, Zhihua Zhou, Handong Li, Haining Ji, Xiaobin Niu, Alexander O Govorov, and Others. Broadband efficiency enhancement in quantum dot solar cells coupled with multispiked plasmonic nanostars. *Nano Energy*, 13:827–835, 2015.

[19] Robert A Taylor, Todd Otanicar, and Gary Rosengarten. Nanofluid-based optical filter optimization for PV/T systems. *Light: Science & Applications*, 1(10):e34, 2012.

[20] Robert A Taylor, Todd P Otanicar, Yasitha Herukerrupu, Fabienne Bremond, Gary Rosengarten, Evatt R Hawkes, Xuchuan Jiang, and Sylvain Coulombe. Feasibility of nanofluid-based optical filters. *Applied optics*, 52(7):1413–1422, 2013.

[21] Robert A Taylor, Patrick E Phelan, Todd P Otanicar, Ronald Adrian, and Ravi Prasher. Nanofluid optical property characterization: towards efficient direct absorption solar collectors. *Nanoscale research letters*, 6(1):225, 2011.

[22] NILT, 2017.

[23] Sohee Kim, Une Teak Jung, Soo Kyoung Kim, Joon Hee Lee, Hak Soo Choi, Chang Seok Kim, and Myung Yung Jeong. Nanostructured multifunctional surface with antireflective and antimicrobial characteristics. *ACS Applied Materials and Interfaces*, 7(1):326–331, 2015.

[24] Alexander B. Christiansen, Jeppe S. Clausen, N. Asger Mortensen, and Anders Kristensen. Injection moulding antireflective nanostructures. *Microelectronic Engineering*, 121:47–50, 2014.

[25] Jeppe S Clausen, Alexander B Christiansen, Anders Kristensen, and N Asger Mortensen. Enhancing the chroma of pigmented polymers using antireflective surface structures. *Applied Optics*, 52(32):7832–7, 2013.

[26] Hwajin Oh, Jaehong Park, Youngseok Song, and Jaeryoun Youn. Microinjection Moulding of Lab-on-a-chip (LOC). 19, 2011.

[27] Usama M. Attia, Silvia Marson, and Jeffrey R. Alcock. Micro-injection moulding of polymer microfluidic devices. *Microfluidics and Nanofluidics*, 7(1):1–28, 2009.

[28] Jasmine P Devadhasan, Sanghyo Kim, and Jeongho An. Fish-on-a-chip: a sensitive detection microfluidic system for Alzheimer's disease. *Journal of biomedical science*, 18(1):33, 2011.

[29] Max Groenendijk. Fabrication of Super Hydrophobic Surfaces by fs Laser Pulses. *Laser Technik Journal*, 5(3):44–47, 2008.